Hydrodynamic and thermodiffusive instability effects on the evolution of laminar planar lean premixed hydrogen flames

C. Altantzis[1], C. E. Frouzakis[1]†, A. G. Tomboulides[2], M. Matalon[3] and K. Boulouchos[1]

[1] Aerothermochemistry and Combustion Systems Laboratory, Swiss Federal Institute of Technology, Zurich, CH-8092, Switzerland

[2] Department of Mechanical Engineering, University of Western Macedonia, 50100 Kozani, Greece

[3] Mechanical Science and Engineering, University of Illinois at Urbana-Champaign, Urbana IL 61801, USA

Numerical simulations with single-step chemistry and detailed transport are used to study premixed hydrogen/air flames in two-dimensional channel-like domains with periodic boundary conditions along the horizontal boundaries as a function of the domain height. Both unity Lewis number, where only hydrodynamic instability appears, and subunity Lewis number, where the flame propagation is strongly affected by the combined effect of hydrodynamic and thermodiffusive instabilities are considered. The simulations aim at studying the initial linear growth of perturbations superimposed on the planar flame front as well as the long-term nonlinear evolution. The dispersion relation between the growth rate and the wavelength of the perturbation characterizing the linear regime is extracted from the simulations and compared with linear stability theory. The dynamics observed during the nonlinear evolution depend strongly on the domain size and on the Lewis number. As predicted by the theory, unity Lewis number flames are found to form a single cusp structure which propagates unchanged with constant speed. The long-term dynamics of the subunity Lewis number flames include steady cell propagation, lateral flame movement, oscillations and regular as well as chaotic cell splitting and merging.

Key words: laminar reacting flows, flames, combustion, instability

1. Introduction

Premixed combustion has been the subject of extensive experimental, theoretical as well as numerical work, concerning both applications and aspects of fundamental interest. The recent progress in computational capabilities has made numerical studies of flames at scales comparable to laboratory experiments feasible, thus increasing their importance in combustion research. Although in most practical applications combustion occurs in a turbulent environment, the study of laminar flames and

† Email address for correspondence: frouzakis@lav.mavt.ethz.ch

the transition to corrugated flames is important for understanding the fundamental mechanisms of turbulent flame propagation and the complex flame–flow interactions involved.

The planar flame, the simplest form of combustion illustrating the propagating nature of premixed flames, is amenable to analysis that provides fundamental understanding of the intrinsic instabilities observed in laboratory experiments; see for example Markstein (1951), Palm-Lewis & Strehlow (1969), Groff (1982), Sivashinsky (1983), Clavin (1985), Bradley *et al.* (2000) and Bradley, Cresswell & Puttock (2001), Law (2006) and Matalon (2007). Excluding acoustic and buoyancy effects, a planar premixed flame can be rendered unstable by hydrodynamic and thermodiffusive mechanisms. The hydrodynamic instability is due to the gas expansion that results from the heat released by the chemical reactions, which induces a flow that tends to convect any flame perturbation further away from the planar shape. Thermodiffusive instabilities result from the disparity of the diffusion rates of heat away from and mass towards the flame.

The destabilizing effect of thermal expansion was discovered by Darrieus (1946) and Landau (1944), who neglected the influences of diffusion, treating the flame as a surface of density discontinuity that propagates into the fresh mixture at a constant speed. The unconditionally unstable conclusion of Darrieus and Landau was recognized to be inconsistent with experimental observations, which led Markstein (1964) to re-examine the stability analysis complementing the assumption regarding the flame speed with a curvature correction, diffusive in nature, and showing that it may introduce stabilizing influences on the short-wavelength disturbances.

Thermodiffusive effects were studied using a flame model which assumes that the flow field is unaffected by the flame, effectively considering constant gas density (Barenblatt, Zeldovich & Istratov 1962; Sivashinsky 1977*b*). In the absence of the hydrodynamic instability, the planar flame was found stable provided the effective Lewis number of the mixture Le_{eff} is near unity; otherwise, due to the disparity of the diffusion rates of heat and mass, instabilities in the form of cells or spontaneous oscillations occur. For mixtures with Le_{eff} sufficiently less than one, the molecular diffusivity of the deficient reactant in the mixture is significantly larger than the thermal diffusivity of the mixture, leading to an intensification of the reaction rate at the convex toward the reactants segments of the flame front and its weakening at the concave parts, and hence to the formation of cells on the flame surface. An oscillatory instability is predicted for mixtures with Le_{eff} sufficiently larger than one, but the predicted critical value of the Lewis number is quite large and inaccessible to common combustible mixtures, except when heat losses are significant.

The coupled effects of hydrodynamic and thermodiffusive instabilities were studied systematically by Frankel & Sivashinsky (1982), Matalon & Matkowsky (1982) and Pelce & Clavin (1982), exploiting the multi-scale nature of the problem characterized by a thin flame with relatively large corrugations and no limitation on the thermal expansion ratio $\sigma \equiv \rho_u/\rho_b$, where ρ_u and ρ_b are the densities of the unburned and burned gas, respectively. These results were later generalized for a two-reactant (fuel and oxidizer) model, allowing for temperature-dependent transport and mixtures ranging from lean to rich conditions (Matalon, Cui & Bechtold 2003). The resulting asymptotic solution is effectively a long wave approximation of the dispersion relation, with the leading term, positive for all σ and proportional to the wavenumber k, describing the Darrieus–Landau instability. The correction terms, of the order of k^2, are the thermodiffusive effects, which have stabilizing influences when Le_{eff} exceeds a critical value Le_{eff}^*, and destabilizing influences otherwise. The critical value Le_{eff}^*

depends on thermal expansion, and for all σ is slightly below one. Short wave stabilization for $Le_{eff} < Le_{eff}^*$ appears only at higher order in k, terms that have not been computed in general, except for the constant density case (Sivashinsky 1977*b*). The instability is thermodiffusive in nature leading to cellular flames characterized by cells of dimensions proportional to the wavelength of the fastest growing mode predicted by the linear stability theory which, as noted, is known only in the limit $\sigma \to 1$. The flame development beyond the instability threshold was studied primarily within the context of a diffusive-thermal model (Michelson & Sivashinsky 1977; Denet & Haldenwang 1992; Kurdyumov *et al.* 2009). Although the early development appears driven by thermodiffusive effects, thermal expansion is likely to play an important role that becomes substantial as the flame grows larger. The formation of cellular flames for realistic values of thermal expansion σ, and the flame development well within the nonlinear regime are some of the objectives of this work.

For $Le_{eff} > Le_{eff}^*$ diffusion effects stabilize short wavelength disturbances, i.e. with wavelength $\lambda < \lambda_c$ (defined below), so that when limited to a finite domain of width $L < \lambda_c$ the planar flame remains absolutely stable. In wider domains, the instability is hydrodynamic in nature. The flame development was studied extensively within the context of the weakly nonlinear Michelson–Sivashinsky equation (Sivashinsky 1977*a*; Michelson & Sivashinsky 1977, 1982; Bychkov 1998; Vaynblat & Matalon 2000*a*,*b*; Karlin 2002), valid for weak thermal expansion, and more recently for realistic values of the thermal expansion within the context of a fully-nonlinear hydrodynamic model (Rastigejev & Matalon 2006*a*,*b*; Creta & Matalon 2011); see also Bychkov & Liberman (2000). In the hydrodynamic model, the flame is treated as an interface propagating at a speed that depends on flame stretch and modulated by a Markstein length, a parameter of the order of the flame thickness that mimics the effects of diffusion, mixture strength and stoichiometry. It has been established that unlike the cellular flames resulting from a thermodiffusive instability, the flame beyond the bifurcation point where the planar flame looses stability evolves into a single cusp-like structure that fills the entire domain L and propagates at a speed significantly larger than the laminar flame speed. It has also been noted that background noise and weak turbulence may trigger self wrinkling of the flame front (Creta, Fogla & Matalon 2011).

The accurate investigation of the interactions between flow, chemistry and transport processes on the initial (linear) as well as the long-term (nonlinear) evolution of the propagating front must take into account the finite flame thickness, and can only be achieved by solving the complete system of the reactive Navier–Stokes equations. Denet & Haldenwang (1995) solved the low Mach number form of the equations in two-dimensional domains and extracted the growth rate that was compared with the dispersion relation of Pelce & Clavin (1982). Good agreement was found at the low wavenumber limit even at relatively low values of the activation energy, but discrepancies were observed when the band of unstable wavenumbers became large for low Lewis numbers. It was further found that the growth rates were not sensitive to viscosity. In a series of papers, Kadowaki studied the influence of the hydrodynamic and the hydrodynamic/thermodiffusive instabilities on planar as well as circular flames over a wide range of Lewis numbers with and without gravitational forces (see the review paper of Kadowaki & Hasegawa (2005) and the references therein). Sharpe (2003) employed a shooting method to investigate the linear stability of planar premixed flames for different values of the activation energy and thermodynamic and transport properties. The comparison with the high activation energy asymptotic expressions showed that for low *Le* the numerical dispersion relation differs from

the theoretical expression. The long-time propagation was numerically simulated in domains with heights equal to approximately six and twelve times λ_{max}, the wave length of the linearly most unstable mode, by Kadowaki, Suzuki & Kobayashi (2005), while Yuan, Ju & Law (2005) and Sharpe & Falle (2006) considered narrower domains (one to three λ_{max} and one to two λ_{max}, respectively). Larger domains of up to $10.6\lambda_{max}$ were considered in (Yuan, Ju & Law 2007).

Interesting dynamic characteristics (cell formation, lateral flame movement, cell splitting and merging in wide domains and stable cellular flame propagation in narrow domains) were identified in these studies, but a systematic investigation of the effect of the domain size and the sequence of transitions leading to the formation of different cellular patterns has not been presented before. It should also be noted that all these works considered transport and thermodynamic properties that did not depend on the local conditions.

The present work is based on highly resolved numerical simulations of the low Mach number reactive Navier–Stokes equations with the chemistry described by an overall one-step reaction and variable thermodynamic and transport properties. The computations were carried out for a hydrogen/air mixture with reaction orders and kinetic parameters specified such that the computed laminar flame speed matches the value obtained with a detailed reaction mechanism. The study addresses both types of instabilities: (i) the thermodiffusive instability, characterized by values of the Lewis numbers representative of the lean hydrogen/air flame, which correspond to an effective Lewis number $Le_{eff} = 0.404$ for the mixture, and (ii) the hydrodynamic instability characterized by unity Lewis numbers for all species. Although the initial flame development is triggered by one of the two instability mechanisms, the nonlinear evolution is subject to both hydrodynamic and thermodiffusive effects with different consequences when the effective Lewis number of the mixture is equal to or significantly below one. In order to control the relative importance of the two instability mechanisms, the simulations were conducted in two-dimensional rectangular domains with variable height. Detailed chemistry and transport effects were incorporated in the recent study of the short- and long-term dynamics of lean premixed hydrogen/air flames at pressure $p = 5$ atm (Altantzis *et al.* 2011). Detailed chemistry simulations of propagating hydrogen flames were also performed by other authors with different objectives. Patnaik *et al.* (1988) showed that the appearance of patterns resembling cellular flames is due to thermodiffusive instability. Grcar, Bell & Day (2009) found significant difference between the results obtained using a mixture-averaged and a multicomponent diffusion model for a propagating lean ($\phi = 0.37$) premixed hydrogen/air flame, while Day *et al.* (2009) studied the effect of turbulence on the cellular burning structures. While the effect of detailed chemistry is not yet clear, the recent study of Sharpe & Falle (2011) with a two-step model taking into account intermediate species into the flame structure found no qualitatively new cellular dynamics than those obtained with single-step models.

The influence of the instability mechanisms on the long-term evolution of a flame front is important since the distortion of the planar geometry induces high propagation velocities and stretch rates. Numerical studies conducted so far on unsteady stretch effects on the propagation characteristics of premixed flames have predominantly considered the turbulent case (e.g. Haworth & Poinsot 1992; Peters *et al.* 1998; Chen & Im 1998; Chakraborty & Cant 2004), while unsteady aerodynamic and curvature effects on the propagation of unstable self-wrinkled laminar flames have not been investigated in detail.

2. Problem setup

2.1. *Governing equations*

At the low-Mach number limit, acoustic wave propagation can be filtered out, and the governing equations can be efficiently integrated while density variations due to heat release and composition variations are fully taken into account (Chu & Kovasznay 1958; Rehm & Baum 1978). The governing equations are the conservation equations for mass, momentum, energy and species together with the equation of state:

Continuity

$$\frac{\partial \rho}{\partial t} + \nabla \cdot (\rho \boldsymbol{u}) = 0. \tag{2.1}$$

Momentum

$$\rho \left(\frac{\partial \boldsymbol{u}}{\partial t} + \boldsymbol{u} \cdot \nabla \boldsymbol{u} \right) = -\nabla p_1 + \nabla \cdot (\mu \boldsymbol{S}) \tag{2.2}$$

$$\boldsymbol{S} = \nabla \boldsymbol{u} + (\nabla \boldsymbol{u})^{\mathrm{T}} - \frac{2}{3} (\nabla \cdot \boldsymbol{u}) \boldsymbol{I}. \tag{2.3}$$

Energy

$$\rho c_p \left(\frac{\partial T}{\partial t} + \boldsymbol{u} \cdot \nabla T \right) = \nabla \cdot (\lambda \nabla T) - \sum_{i=1}^{N_g} h_i \dot{\omega}_i - \rho \left(\sum_{i=1}^{N_g} c_{p,i} Y_i V_i \right) \cdot \nabla T \tag{2.4}$$

$$c_p = \sum_{i=1}^{N_g} c_{p,i} Y_i. \tag{2.5}$$

Species

$$\rho \left(\frac{\partial Y_i}{\partial t} + \boldsymbol{u} \cdot \nabla Y_i \right) = -\nabla \cdot (\rho Y_i V_i) + \dot{\omega}_i \quad i = 1, \dots, N_g \tag{2.6}$$

Equation of state (ideal gas law)

$$p_0 = \rho R T / \bar{W}. \tag{2.7}$$

In the low-Mach-number formulation, equation (2.1) is replaced by (2.8) below, which is obtained by combining the continuity (2.1), energy (2.4), species (2.6) and state (2.7) equations:

$$\nabla \cdot \boldsymbol{u} = -\frac{1}{\rho} \left(\frac{\partial \rho}{\partial t} + \boldsymbol{u} \cdot \nabla \rho \right) = \frac{1}{\rho} \sum_{i=1}^{N_g} h_i \frac{\bar{W}}{W_i} (-\nabla \cdot \rho Y_i V_i + \dot{\omega}_i)$$

$$+ \frac{1}{\rho c_p T} \left[\nabla \cdot (\lambda \nabla T) - \sum_{i=1}^{N_g} h_i \dot{\omega}_i - \rho \left(\sum_{i=1}^{N_g} c_{p,i} Y_i V_i \right) \cdot \nabla T \right]. \tag{2.8}$$

In (2.1)–(2.8), $h_i, \dot{\omega}_i, Y_i, V_i, W_i, c_{p,i}$ are the enthalpy, chemical production term, mass fraction, diffusion velocity, molecular weight, and heat capacity of species i, respectively, while λ is the thermal conductivity, p_1 and p_0 the so-called 'hydrodynamic' and the 'thermodynamic' pressures, $\bar{W}$ the mean molecular weight and c_p the mixture heat capacity. We use $\boldsymbol{I}$ to denote the identity matrix and the species diffusion velocities V_i are given by Fick's law

$$V_i = -(D_i / X_i) \nabla X_i, \tag{2.9}$$

D_i and $X_i = Y_i W_i / \bar{W}$ being the *i*th species mixture-averaged diffusivity and mole fraction, respectively. Pressure diffusion, thermal diffusion and body forces are not taken into account.

2.2. *Computational domain and solution method*

The equations are discretized in space using the spectral element method (Patera 1984; Deville, Fischer & Mund 2002) in a computational domain that is split into rectangular conforming elements. The solution, data and geometry are expressed as sums of tensor products of order N_p Legendre polynomials based on the Gauss–Lobatto–Legendre quadrature points. The discretized equations are solved with a parallel code based on the incompressible flow solver *nek*5000 (Fischer, Lottes & Kerkemeier 2008) using a high-order splitting scheme for low-Mach-number reactive flows (Tomboulides, Lee & Orszag 1997). A semi-explicit integration scheme is used for the continuity and momentum equations, while the energy and species equations are solved implicitly using CVODE (Byrne & Hindmarsh 1999). Further details on the mathematical formulation, the numerical method as well as validation of the approach along with asymptotic analysis and numerical benchmark tests can be found in Tomboulides *et al.* (1997) and Tomboulides & Orszag (1998).

We consider a lean premixed H_2/air mixture with equivalence ratio $\phi = 0.6$, at temperature and pressure equal to $T = 298$ K and $p = 5$ atm, respectively. The chemistry is described by the single-step global reaction

$$H_2 + 0.5 O_2 \rightarrow H_2O \tag{2.10}$$

with the following reaction rate expression

$$r = A \exp\left(-\frac{E_a}{RT}\right) [H_2]^a [O_2]^b . \tag{2.11}$$

According to Sun *et al.* (1999), at $\phi = 0.6$ the reaction orders with respect to H_2 and O_2 are $a = 1.6$ and $b = 0.1$, respectively, while the activation energy is $E_a = 40.3$ kcal mol^{-1}. The pre-exponential factor A was adjusted so that the laminar flame speed computed with the PREMIX code (Rupley, Kee & Miller 1995) from Chemkin's suite matches the value of $S_L = 51.4$ cm s^{-1} obtained with the detailed mechanism of Li *et al.* (2004). Detailed transport properties using the mixture-averaged formulation are computed using the Chemkin transport library (Kee *et al.* 1996*a*), while the thermodynamic properties and chemical reaction rate are evaluated with Chemkin (Kee, Rupley & Miller 1996*b*). The planar flame thickness is related to the adiabatic flame temperature T_b, the unburned mixture temperature T_u and the maximum temperature gradient in the one-dimensional flame as

$$\delta_T = \frac{T_b - T_u}{\max(dT/dx)}, \tag{2.12}$$

and defines the reference length scale. Using the laminar flame speed as the reference velocity, the reference time is defined as $t_{ref} = \delta_T / S_L$.

The Lewis numbers of the fuel and oxidizer in the fresh mixture are $Le_{H_2} = 0.39$ and $Le_{O_2} = 1.62$, respectively. For the actual values of *Le*, the pre-exponential factor was found to be $A = 1.077 \times 10^{16}$ (mol cm^{-3})$^{-0.7}$ s^{-1}, the adiabatic flame temperature was $T_b = 1839.5$ K and the flame thickness was $\delta_T = 5.14 \times 10^{-3}$ cm, resulting in a Zel'dovich number, expansion coefficient and Prandtl number equal to $\beta = E_a(T_b - T_u)/(RT_f^2) = 9.235$, $\sigma = \rho_u / \rho_b = 6.173$ and $Pr = 0.506$, respectively.

In order to isolate the effect of hydrodynamic instability on the propagation of the planar front, unity Lewis number flames were also simulated by setting the species diffusivities equal to the thermal diffusivity. In the unity Le case, the corresponding values are $A = 2.087 \times 10^{15}$ (mol cm^{-3})$^{-0.7}$ s^{-1}, $T_b = 1848.1$ K, $\delta_T = 5.74 \times 10^{-3}$ cm, $\beta = 9.205$, $\sigma = 6.201$ and $Pr = 0.506$.

The simulations were performed in two-dimensional rectangular domains with fixed length equal to $200\delta_T$ and height ranging from $3\delta_T$ to $80\delta_T$. In the following, the corresponding cases will be referred to as h_H, where H denotes the domain height in units of δ_T. Around the flame, uniform quadrilateral elements with $\delta_x = \delta_y = 0.5\delta_T$ and polynomial order $N = 10$ in each direction were used so that the flame thickness is resolved with 21 grid points, corresponding, for the $Le_{eff} < 1$ case, to a resolution of approximately 2.45 μm, and for the $Le_{eff} = 1$ case of 2.73 μm. At the inflow (left boundary), Dirichlet boundary conditions are used for the velocity (uniform profile with $u_{in} = S_L$) and temperature ($T_{in} = 298$ K), and flux boundary conditions for the species mass fractions. Zero-Neumann boundary conditions were prescribed for all variables at the outflow (right boundary), while periodicity was imposed along the top and bottom horizontal boundaries. In order to minimize boundary effects, the planar flame profile obtained using PREMIX was placed at $x = 130\delta_T$ and the flame evolution was followed until $x = 60\delta_T$. Furthermore, since the employed low-Mach-number formulation does not suffer from acoustic wave reflections at the inflow and outflow boundaries, the domain does not need to be as large as with fully compressible solvers. It should be noted that in narrow domains where the flame is stable, the one-dimensional solution remained stationary during long time integration, and the highly resolved solution of PREMIX could be accurately reproduced with only eight points within the flame thickness. In order to further check the resolution independence of the solution, some simulations were repeated with lower polynomial orders. It was found that the linear and nonlinear behaviour as well as the sequence of dynamics were unaffected when the δ_T was resolved by 12 points.

Unless otherwise noted, all variables reported below are non-dimensionalized with respect to δ_T, S_L, t_{ref}, T_{in} and the properties of the inflowing mixture.

2.3. *Theoretical considerations*

The analysis of Matalon *et al.* (2003) assumes that the mixture consists of two reactants, fuel and oxidizer, with the chemistry described by a single-step overall reaction characterized by an activation energy and arbitrary reaction orders. The flame is assumed thin in comparison to the hydrodynamic length scale, transport properties vary with temperature and density varies throughout the flame. In examining the stability of a planar flame front they derived a dispersion relation expressing the growth rate ω as a function of the perturbation wavenumber k, which in dimensionless form reads

$$\omega = \omega_0 k - \delta[B_1 + \beta(Le_{eff} - 1)B_2 + PrB_3]k^2, \tag{2.13}$$

where ω_0, B_1, B_2 and B_3 are functions only of the thermal expansion coefficient σ. To accommodate the different characteristic length used in this paper, the coefficient multiplying the second-order term on the right-hand side must be defined as $\delta = \delta_T/l_{th}$, where

$$l_{th} = \frac{\lambda_u}{\rho_u c_p S_L}. \tag{2.14}$$

The scaling is $\delta = 4.1$ and 3.7 for the unity and subunity Lewis number cases, respectively. The coefficients appearing in (2.13) are

$$\omega_0 = \frac{\sqrt{\sigma^3 + \sigma^2 - \sigma} - \sigma}{\sigma + 1} \tag{2.15}$$

$$B_1 = \frac{\sigma}{2} \left[\frac{\sigma(2\omega_0 + \sigma + 1)}{(\sigma - 1)[\sigma + (\sigma + 1)\omega_0]} \int_1^\sigma \frac{\lambda(x)}{x} \, dx + \frac{1}{\sigma + (\sigma + 1)\omega_0} \int_1^\sigma \lambda(x) \, dx \right] \tag{2.16a}$$

$$B_2 = \frac{\sigma}{2} \left[\frac{(1 + \omega_0)(\sigma + \omega_0)}{(\sigma - 1)[\sigma + (\sigma + 1)\omega_0]} \int_1^\sigma \ln\left(\frac{\sigma - 1}{x - 1}\right) \frac{\lambda(x)}{x} \, dx \right] \tag{2.16b}$$

$$B_3 = \frac{\sigma}{2} \left[\frac{2(\sigma - 1)}{\sigma + (\sigma + 1)\omega_0} \lambda(\sigma) - \frac{2}{\sigma + (\sigma + 1)\omega_0} \int_1^\sigma \lambda(x) \, dx \right] \tag{2.16c}$$

where $\lambda(x)$ expresses the variation of the transport properties with temperature, and Le_{eff} is the effective Lewis number defined below. Although derived for a general functional dependence $\lambda(T)$, the stability results were presented in Matalon *et al.* (2003) only for the special case $\lambda = T$ (without being explicitly stated) and with a minor typo in the coefficient B_2 (there is an extra factor $\sigma - 1$ in the numerator). For constant transport properties, $\lambda = 1$, and these relations reduce to those derived by Frankel & Sivashinsky (1982), Matalon & Matkowsky (1982) and Pelce & Clavin (1982) when the different notation used in these publications is properly accounted for.

The first-order term in (2.13) $\sim k$ expresses the growth due to the Darrieus–Landau instability (since $\omega_0 > 0$ for all σ), while the second-order term $\sim k^2$ represents the influences of diffusion with the coefficients B_1, B_2 and B_3 corresponding to thermal conduction, mass diffusion and viscosity effects, respectively. Since $\sigma > 1$, B_1, B_2 and B_3 are always positive, the terms expressing thermal conduction and viscous diffusion are always stabilizing, while mass diffusion can be stabilizing or destabilizing depending on the effective Lewis number of the mixture. When $Le_{eff} < 1$, the mass diffusion term becomes negative and plays a destabilizing role. The combined diffusion terms, therefore, act to destabilize the flame when $Le_{eff} < Le_{eff}^*$, with the critical value Le_{eff}^* obtained by setting $\omega = 0$ in (2.13), is slightly less than one. It should be noted that the increase in viscosity that results from the increase in temperature across the flame has a stabilizing effect on the flame, and when the viscosity is assumed constant and independent of temperature, the coefficient $B_3 = 0$ and viscous effects play a secondary role compared with all other diffusion effects.

The dispersion relation (2.13) was used for comparison with the data obtained from the simulations. The fit of the thermal conduction coefficient profile along the one-dimensional solution of PREMIX by a power-law expression showed that $\lambda = T^{0.7}$. The effective Lewis number of the fresh mixture is

$$Le_{eff} = \frac{Le_E + Le_D A}{1 + A} \tag{2.17}$$

$$A = \frac{G(a, b; \varphi)}{bG(a, b - 1; \varphi)} - 1 \tag{2.18}$$

$$G(a, b; \varphi) = \int_0^\infty \varsigma^a (\varsigma + \varphi)^b e^{-\varsigma} \, d\varsigma \tag{2.19}$$

$$\varphi = \beta(\Phi - 1), \tag{2.20}$$

where $\Phi = \phi^{-1}$ when $\phi < 1$ and $\Phi = \phi$ for $\phi > 1$, with ϕ the equivalence ratio and a and b the reaction orders of the excess and the deficient reactant, denoted by the subscripts E and D, respectively. For the conditions considered, $Le_{eff} = 0.404$, which is very close to the fuel Lewis number ($Le_{H_2} = 0.39$) as expected for lean mixtures.

The asymptotic relation (2.13) is in fact the expansion of the exact dispersion relation in powers of k. For $Le_{eff} < Le_{eff}^*$, when both coefficients in the expansion become positive, stabilization at large k comes from higher-order terms which have not been derived under general conditions. They are included, however, in the dispersion relation obtained by Sivashinsky (1977b) when considering only thermodiffusive instability and ignoring the effects of thermal expansion and viscosity, thus effectively setting $\sigma = 1$. The implicit dispersion relation in that case takes the form

$$F(\omega, k, Le) = \frac{(Le - q)(p - r)}{Le - q + p - 1} - \frac{\beta}{2}, \tag{2.21}$$

where, accounting for the different reference length scale,

$$p = \frac{1}{2}\left[1 + \sqrt{1 + 4(\delta\omega + \delta^2 k^2)}\right] \tag{2.22}$$

$$q = \frac{Le}{2}\left[1 + \sqrt{\frac{1 + 4(\delta\omega Le + \delta^2 k^2)}{Le^2}}\right] \tag{2.23}$$

$$r = \frac{1}{2}\left[1 - \sqrt{1 + 4(\delta\omega + \delta^2 k^2)}\right]. \tag{2.24}$$

In the work of Sivashinsky (1977b), the hydrodynamic problem is separated from the reaction–diffusion problem, and the only factors considered are heat conduction and mass diffusion. Consequently, the stability properties of the planar flame front depends only on the Lewis and Zel'dovich numbers.

2.4. *Flame stretch and flame speed*

In the simulations presented below the flame front was identified by a temperature isoline and the results processed to compute linear growth rates, as well as flame speeds, curvature, strain rate, and flame stretch. The instantaneous fronts were decomposed into their Fourier components and the evolution of the dominant modes was followed in time. The linear growth rate of each Fourier mode was obtained from the slope of the temporal variation of the logarithm of the growth.

The flame speed can be defined in different ways (Poinsot & Veynante 2005). The 'local displacement speed', i.e. the flame front speed relative to the flow, is defined as

$$S_d = \frac{1}{|\nabla T|}\left[-\sum_{i=1}^{N_g} h_i \dot{\omega}_i + \nabla \cdot (\lambda \nabla T) - \rho \left(\sum_{i=1}^{N_g} c_{p,i} Y_i V_i\right) \cdot \nabla T\right] \tag{2.25}$$

with all quantities evaluated along the temperature isoline chosen to define the flame front. It takes into account the heat release rate (HRR; first term in the brackets) and the heat flux (the last two terms representing the heat conduction term and the heat transfer through species diffusion, respectively). The last term which is identically zero when the heat capacities of the species are equal is found to be orders of magnitude smaller than the other two terms. As will be shown below, the incorporation of the heat flux in the definition of the local flame speed is necessary in order to understand the evolution of the front. Flame speed definitions such as the local consumption speed

are based solely on the local reactivity (Poinsot & Veynante 2005), and cannot be used to explain the behaviour of wrinkled flames propagating in non-uniform flows.

The 'absolute propagation velocity', the propagation velocity of the flame front with respect to the fixed laboratory frame of reference, is $w = S_d n + u$, where $n = -\nabla T / |\nabla T|$ is the local flame normal vector pointing towards the fresh mixture and u the local flow velocity.

Wrinkling of the flame front affects the local reactivity through the thermodiffusive effect, the heat conduction from the reaction zone to the unburned mixture, and the flow non-uniformity through the hydrodynamic instability. The first two effects are induced by the front curvature, while the latter is expressed by the strain rate. The combined effect of curvature and strain is the stretch rate. Curvature is defined as the divergence of the flame normal vector n,

$$\kappa = \nabla \cdot n. \tag{2.26}$$

Flame stretch can be obtained using the computationally convenient expressions (Matalon 1983; Chung & Law 1984; Candel & Poinsot 1990),

$$K = \frac{1}{A}\frac{\mathrm{d}A}{\mathrm{d}t} = a_t + S_d \kappa \tag{2.27a}$$
$$= -n \cdot \nabla \times (u \times n) + (w \cdot n)(\nabla \cdot n), \tag{2.27b}$$

where A is the flame area and the total aerodynamic strain rate of the flame front is (Williams 1985)

$$a_t = (\delta_{ij} - n_i n_j)\frac{\partial u_i}{\partial x_j}. \tag{2.28}$$

The first term in (2.27b) expressing the tangential strain rate is equal to the divergence of the tangential flow velocity

$$\nabla \cdot u_t = \nabla_t \cdot u_t = -n \cdot \nabla \times (u \times n) = a_t - (u \cdot n)\nabla \cdot n. \tag{2.29}$$

The normal strain acting on the flame surface (last term of (2.29)) depends on flame curvature through the modification of n with respect to the Cartesian frame of reference. The normal and tangential strain rates counteract each other, so that negatively curved (concave towards the fuel) regions experience compressive (i.e. negative) tangential strain and expansive (i.e. positive) normal strain. The opposite occurs along positively curved (convex) regions. The tangential strain rate obtained by subtracting the normal strain rate from the total aerodynamic strain rate, incorporates the effects of both aerodynamic strain and curvature. The effect of normal and tangential straining on the propagation of the flame has been recently discussed by Creta & Matalon (2011). The relation of the flame displacement speed with stretch rate and curvature as well as the individual contribution of each of the terms constituting the flame stretch will be examined below for the two cases considered, unity and sub-unity Lewis numbers.

With respect to the effect of heat conduction on S_d and its dependence on curvature, the decomposition of the heat conduction into contributions in the normal and tangential directions

$$\nabla \cdot (\lambda \nabla T) = \partial_n(\lambda \partial_n T) + \nabla_t \cdot (\lambda \nabla_t T)$$
$$= -n \cdot \nabla(\lambda|\nabla T|) - \lambda|\nabla T|(\nabla \cdot n) \tag{2.30}$$

clearly shows the explicit dependence of heat conduction in the tangential direction (and thus of the displacement speed) on curvature.

3. Results and discussion

3.1. *Linear stability of the flame*

Linear stability analysis provides the range of unstable wavenumbers, the maximum amplification rate and the most unstable wavenumber, and as such allows for direct comparison of the numerical results with theoretical predictions. It also furnishes useful information in understanding the formation of cellular structures during the long-time flame propagation.

For most of the domain heights simulated, two types of initial conditions were considered. First, in order to avoid mode locking on the initial perturbation wavelength, the response of the flame to the omnipresent numerical noise was followed in time. At the employed resolution, the noise amplitude is very low (and its amplification requires correspondingly long times), but its spectrum spans an extended range. In addition to this 'self-excitation', the planar front was perturbed into a sinusoidal shape $\Delta = A_0 \sin(k_n y)$, where A_0 is the initial perturbation amplitude and k_n is the wavenumber $k_n = 2\pi n/h$, $n = 1, 2, \ldots$. The comparison of the growth rates obtained with the two approaches showed that for the thermodiffusively unstable flame a value of $A_0 = 0.001$ resulted in growth rates that were very close to each other with the largest deviation (from the unperturbed case) being 2.6 % for the h_6 domain. In the $Le_{eff} = 1$ cases where the growth rates are much lower, the amplitude of the initial perturbation magnitude was taken as $A_0 = 0.1$. Comparison with growth rates obtained using $A_0 = 0.001$ for the h_{10} case showed negligible differences.

The growth rates ω extracted from the simulations are plotted in figure 1(*a*) as a function of the wavenumber k for both Lewis numbers and compared with the theoretical dispersion relations of Landau (1944), Sivashinsky (1977*b*) and Matalon *et al.* (2003).

3.1.1. *Hydrodynamically unstable flames*

For the conditions considered in this study, the critical Lewis number obtained by setting the coefficient of the second-order term in (2.13) equal to zero is $Le_{eff}^* = 0.547$, so that for $Le_{eff} > 0.547$ the theoretical expression is able to capture the stabilizing effect of diffusive processes at high wavenumbers. On the other hand, the theoretical dispersion relation diverges when $Le_{eff} < 0.547$ and high-wavenumber stabilization cannot be predicted.

When the species diffusivities are forced to be equal to the thermal diffusivity, the maximum growth rate of the resulting $Le_{eff} = 1$ flames is $\omega_{max} = 0.202$ at the most unstable wavenumber of $k_{max} = 0.314$ ($h = 20\delta_T$), whereas the neutral stability wavenumber is $k_c = 0.692$ corresponding to a wavelength of $h \approx 9\delta_T$. The numerical results in this case can be compared with the theoretical predictions (2.13) because for unity Lewis numbers $Le_{eff} > Le_{eff}^*$ and, indeed, there is very good agreement for $k < 0.16$. For higher wavenumbers, the agreement is still qualitatively good, but deteriorates gradually for $k > 0.2$. Similar discrepancies were reported by Denet & Haldenwang (1995), Yuan *et al.* (2007) and Sharpe (2003) who compared computed growth rates with the equivalent theoretical predictions (albeit with constant thermodynamic and transport properties) of Pelce & Clavin (1982), Matalon & Matkowsky (1982) and Frankel & Sivashinsky (1982).

The worsening agreement for high wavenumbers suggests that terms of order higher than second in k in the dispersion relation become increasingly important. Since for $Le_{eff} = 1$ flames the thermodiffusive instability plays no role, high-wavenumber stabilization can only be due to diffusion. The higher-order terms would most likely correspond to the combined effects of viscosity, thermal conduction or mass diffusion.
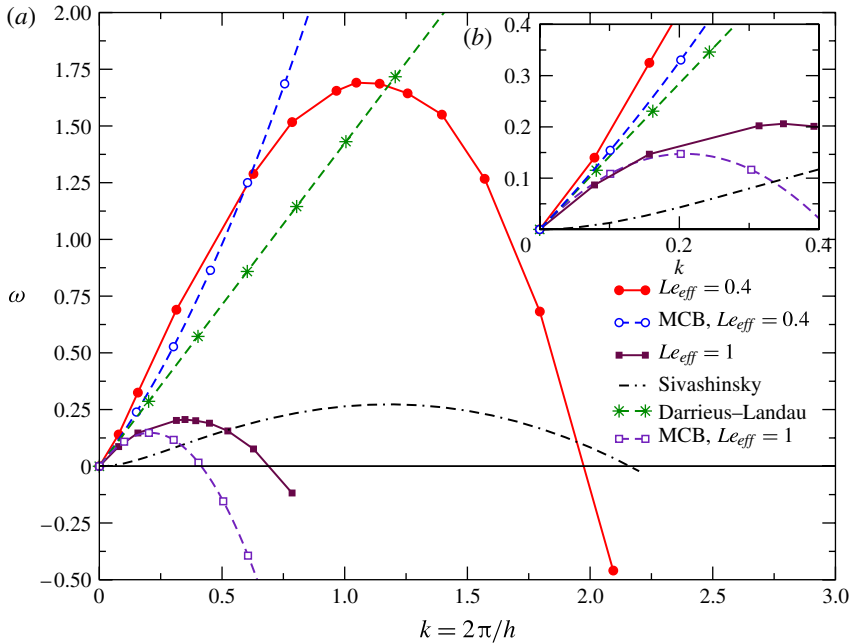
FIGURE 1. (Colour online available at journals.cambridge.org/flm) (*a*) Comparison of the dispersion relation extracted from the simulations for unity as well as low Le_{eff}, with the theoretical expressions of Matalon *et al.* (2003) (MCB, for both Le_{eff} cases), and Sivashinsky (1977*b*) (for $Le_{eff} = 0.404$). (*b*) Expanded view at the low-wavenumber limit.

Considering constant transport properties, Denet & Haldenwang (1995) found that viscosity has a minor effect for $Le_{eff} = 1$ flames, but as noted by Matalon *et al.* (2003) when viscosity is allowed to vary with temperature, its effect is comparable to other diffusion effects.

3.1.2. *Thermodiffusivelly and hydrodynamically unstable flames*

When realistic transport is considered, the effective Lewis number of the lean hydrogen/air mixture ($\phi = 0.6$) becomes $Le_{eff} = 0.404 < Le_{eff}^*$, and the range of unstable modes and the growth rates is more than doubled (figure 1*a*). The neutral stability wavenumber $k_c = 1.974$ (corresponding to $h_c = 3.183\delta_T$) is assessed through linear interpolation between the perturbation wavenumbers $k = 2.094$ ($h = 3\delta_T$) and $k = 1.795$ ($h = 3.5\delta_T$) whose growth rates are negative and positive, respectively. Stabilization of smaller wavelength perturbations is due to the effects of transverse mass diffusion and heat conduction at small scales. The maximum growth rate is $\omega_{max} = 1.691$, corresponding to a most unstable wavenumber $k_{max} = 1.105$ ($h = 6\delta_T$).

Although the ω–k curves for the two cases ($Le_{eff} = 0.404$ and 1) differ significantly, they both tend to the Darrieus–Landau limit when $k \rightarrow 0$, as shown in the close up limited to low wavenumbers (figure 1*b*). Furthermore, an inflection point appears between $k = 0.157$ and $k = 0.314$ (corresponding to the domains h_{40} and h_{20}, respectively) in the low Le_{eff} case. This confirms the assertion that for low Lewis number the asymptotic approximation (2.13) is inadequate and the expansion of the dispersion relation must include terms corresponding to orders higher than k^2. A nonlinear fit of the simulation data with a polynomial expression containing only first-,
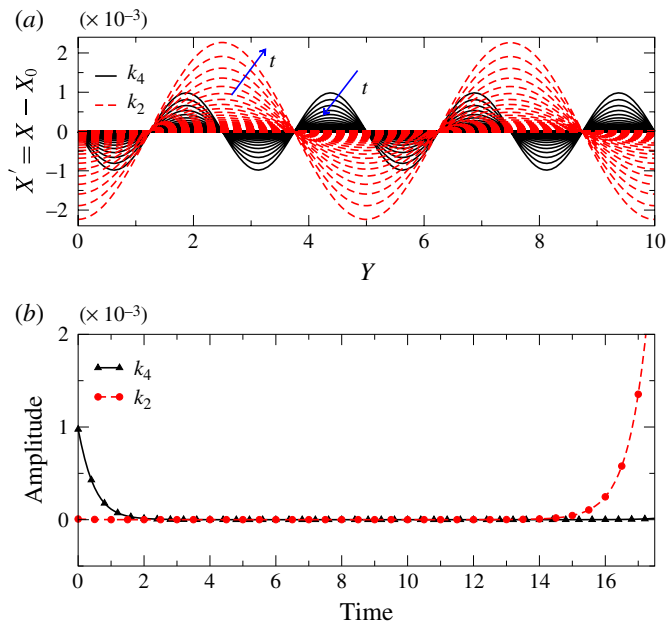
FIGURE 2. (Colour online) (*a*) Evolution of the flame front defined by the $T = 3$ isoline at times differing by one time unit; (*b*) time history of the amplitudes of the k_4 (initial perturbation to a four-cell structure, amplitude decreasing in time) and k_2 (two-cell structure, amplitude increasing in time) Fourier modes.

second- and fourth-order terms in k yields $\omega = 2.641k - 0.884k^2 - 0.111k^4$, with a stabilizing term of the order k^4.

Although the implicit dispersion relation (2.21) of Sivashinsky (1977*b*) does not correctly predict the behaviour near $k = 0$ (being limited to $\sigma = 1$), it does account for higher-order wavenumber effects. The neutral stability wavenumber from the simulations is in reasonable agreement with the value of k_c=2.14 obtained from (2.21). On the other hand, the growth rates extracted from the simulations are larger than the predicted values by a factor that is close to the thermal expansion coefficient. If ω in (2.21) is rescaled to take into account the actual value of the thermal expansion coefficient, effectively substituting ω by ω/σ, the magnitudes of the growth rates are matched quite well.

In order to compare the growth rates of different modes, perturbations of wavelength $\lambda < h$ were also imposed in some cases. The simulations with perturbation wavelengths of $\lambda = h, h/2, h/4$ in the h_{10} domain (corresponding to $k_1, k_2 = 2k_1, k_4 = 4k_1$), and $\lambda = h/2, h/3, h/4$ (k_2, k_3, k_4 modes) in the h_{20} domain showed that the linear growth rates of specific wavelengths are independent of the domain height. For example, the growth rate of the $\lambda = h/2$ mode in the h_{20} domain was found to be equal to that of the $\lambda = h$ mode in the h_{10} domain.

In the h_{10} case, the initial temporal evolution of the displacement of the flame front defined by the $T = 3$ isoline shows that the k_4 mode is damped quickly, while the k_2 mode is amplified slowly and after the initial transient the flame acquires an almost planar shape (figure 2*a*). This can be more clearly seen in figure 2(*b*) showing the time history of the amplitudes of the k_2 and k_4 Fourier modes of the flame front; all other modes had negligible amplitude. The damping of the initial k_4 perturbation

is expected since, according to the numerical dispersion relation, its wavenumber lies outside the instability range. The perturbed flame initially reverts to the planar shape; however, due to the intrinsic instability of the k_2 mode, two cells emerge after some time with wavelength equal to $\lambda = 5\delta_T$. The amplitude of the k_2 mode grows exponentially in time with a growth rate equal to that obtained from the numerical dispersion relation (figure 1a). In all cases considered, the number of cells appearing initially is equal to the integer multiple of the mode with the highest growth rate that can be accommodated in the domain.

3.2. *Nonlinear evolution*

The perturbation imposed on the flame front creates convex (flame crests) and concave (flame troughs) towards the fresh mixture segments along the flame front. The resulting modification of the flow field ahead of the flame leads to divergence/convergence of the streamlines upstream of the crest/trough. The flow-induced stretch, in turn, flattens the region around the crest at the expense of the trough. When the domain height is such that $k_1 < k_c$, the perturbation is amplified, the flame speed becomes larger than S_L and the front propagates towards the inlet. After an initial period of linear growth, different modes can get excited and interact nonlinearly.

Narrow domains are characterized by the strong stabilizing effect of viscosity, transverse heat conduction and mass diffusion and result in a single-cusp flame structure directly. More interesting dynamics are observed in wider domains, where diffusive processes weaken and additional modes can be excited, leading to the appearance of smaller cells along the flattened convex flame segment.

3.2.1. *Hydrodynamically unstable flames*

As shown in figure 3(a,b) for $h \leqslant 20\delta_T$, the flame front defined by the $T = 3$ isoline evolves into a single-cusp structure with a depth increasing with h. Once this stable front shape is acquired, the flame propagates without changing shape towards the unburned mixture with a constant velocity higher than S_L. The speed of the stably propagating flame front with respect to the stationary laboratory frame of reference will be referred to in the rest of the text as the 'global propagation rate', S_A. On the other hand, the propagation speed with respect to the incoming fresh mixture velocity will be called the 'global displacement rate', $S_D = S_A + u_{in}$.

In the wide domains (h_{40} and h_{80} shown in figure 3(c,d), respectively), the initially perturbed k_1 mode is amplified and, after saturation, single-cusp structures are obtained, characterized by an extended low-curvature crest which becomes susceptible to secondary instabilities. In all cases, the smaller structures formed on the crest move along the front and disappear at the trough restoring the single-cusp shape. In order to investigate the influence of noise on flame behaviour, simulations in the wide domains were also performed with lower resolution. The disturbances were sustained for longer times but eventually the flame always acquired a single-cusp shape similar to the thin flame predictions of Rastigejev & Matalon (2006a) and Creta & Matalon (2011).

The temporal evolution of the leading Fourier modes together with the corresponding curves for the temporal evolution of the integral of the non-dimensional HRR (integral $HRR = \int_V \sum_{k=1}^N \dot{\omega}_k h_k \, dV/(t_{ref}^{-1} \rho_{ref} c_{p,ref} T_{ref})$) over the whole domain are plotted in figure 4. The dominance of the k_1 mode, observed in all cases, clearly shows the tendency of the flame to propagate with a single-cusp shape. Only in the h_{40} domain, structures of wavelength k_2 appear and their amplitude temporarily exceeds that of the k_1 mode (figure 4c). This may be attributed to the fact that
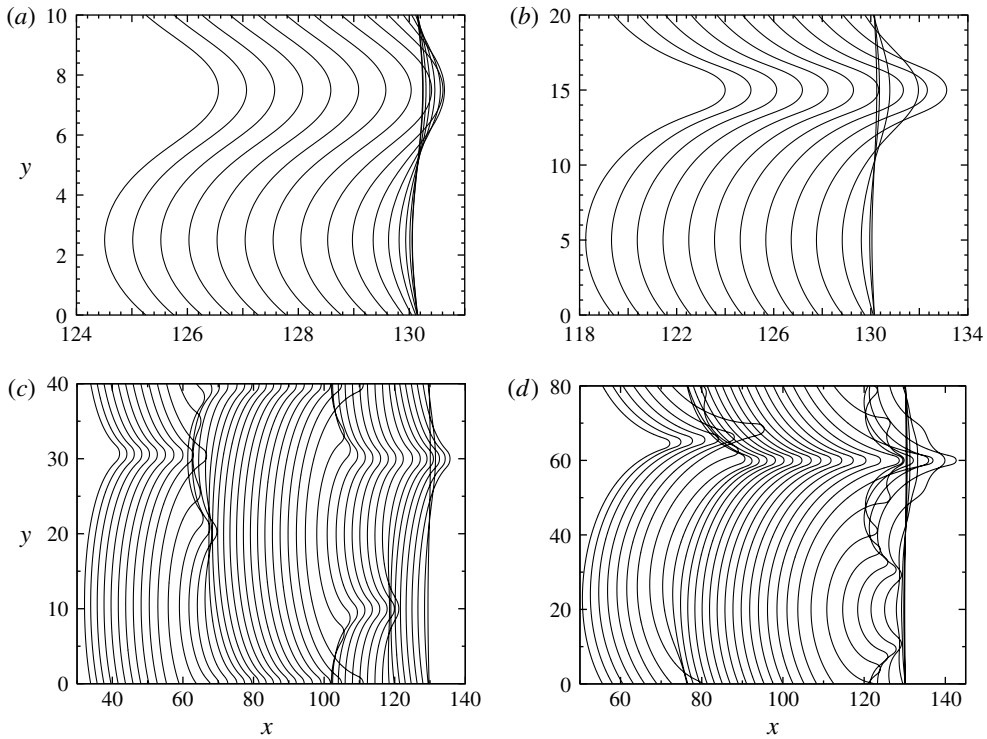
FIGURE 3. Propagation of the flame front defined by the $T = 3$ isoline at times differing by 5 time units in the (a) $h = 10\delta_T$, (b) $h = 20\delta_T$, (c) $h = 40\delta_T$ and (d) $h = 80\delta_T$ domains.

the secondary modes of wavelength $\lambda = 20\delta_T$ were found to exhibit the maximum amplification in the linear stability analysis. In the h_{80} case, the k_1 mode remains dominant throughout the whole simulation time. The temporal evolution of HRR directly reflects the transient formation of smaller structures along the flame front (increase of HRR) as well as the merging of the small-scale structures (decrease of HRR).

The propagation characteristics of the single-cusp flames propagating with a constant velocity and without changing shape are exemplified by the analysis of the h_{10} case (figure 5). The normal component of the local absolute propagation velocity, which will be referred to as the *absolute propagation speed*, $S_a = S_d + \boldsymbol{u} \cdot \boldsymbol{n}$, the density-weighted displacement speed $\hat{S}_d = \rho S_d / \rho_u$, and the curvature κ along the flame front defined by the $T = 1.15$ (close to the upstream boundary of the preheat zone) and $T = 3$ isolines, are extracted at $t = 80$, after the flame has acquired its steady structure.

The density-weighted displacement speed corrects S_d for volumetric expansion effects and can be directly compared with S_L indicated by the straight line $\hat{S}_d = 1$ in figure 5(b). At the leading (flame crest) and trailing (flame trough) points of the front where the flame normal aligns with the streamwise direction, the tangential velocity is zero and the absolute propagation speed is equal to the global propagation rate. It reaches its maximum value $S_a = 0.1$ at the leading and trailing points, and its minimum at the points of zero curvature (marked by the vertical dashed and dotted lines for the $T = 3$ and $T = 1.15$ isoline, respectively) where the angle between the
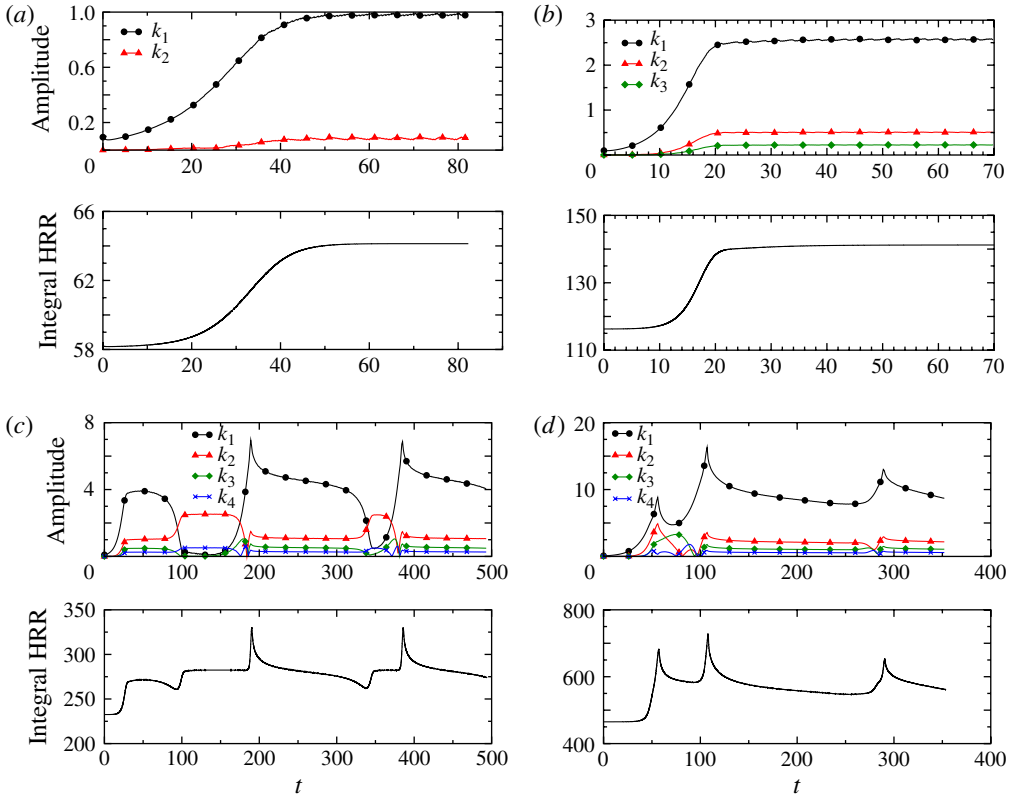
FIGURE 4. (Colour online) Temporal evolution of the amplitude of the first few Fourier modes of the flame shape and of the heat release rate (HRR) in the (*a*) h_{10}, (*b*) h_{20}, (*c*) h_{40}, (*d*) h_{80} domains.

streamwise and the normal direction becomes the largest. As expected, the value of the global propagation rate is independent of the temperature isoline chosen to define the front. The effect of curvature on the density-weighted displacement speed can be inferred from figure 5(*b*,*c*). Positively-curved regions are characterized by $\hat{S}_d < S_L$, while at negatively curved regions $\hat{S}_d > S_L$; only at points of zero curvature, $\hat{S}_d = S_L$.

Since $Le = 1$, the mass diffusing in the reaction zone compensates for the heat loss via conduction to the fresh mixture. As a result, reactivity remains constant along the flame, and the main term contributing to the variation of the displacement speed in (2.25) is thermal conduction, which depends on curvature (equation (2.30)). The variation of heat conduction (*HC*) along the flame front is plotted in figure 5(*d*) for the stable single-cell as well as for the planar frame in the h_{10} domain. Heat conduction upstream from the reaction zone along the convex ($\kappa > 0$) segment of the front is weaker than that of the planar front; the opposite occurs along the $\kappa < 0$ region. The normal, $HC_n = \partial_n(\lambda \partial_n T)$, and tangential components, $HC_t = \nabla_t \cdot (\lambda \nabla_t T)$, of *HC* are plotted in figure 5(*e*,*f*), respectively. The higher values of HC_n in negatively-curved regions reflect the focusing effect which transfers heat from a larger flame surface area to preheat the unburned mixture engulfed in these regions. The explicit dependence of HC_t on curvature (equation (2.30)) explains its variation along the flame (figure 5*f*). In $\kappa > 0$ segments, $HC_t < 0$ since heat is conducted away from these regions towards
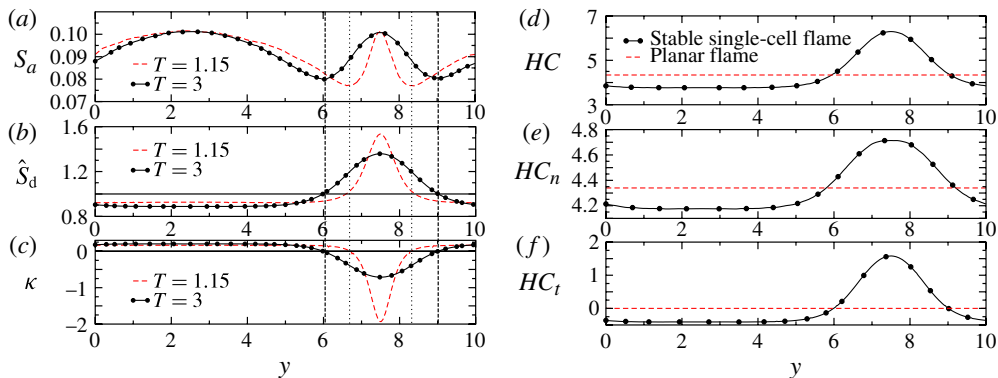
FIGURE 5. (Colour online) Unity *Le* flame in the h_{10} domain: (*a*) absolute propagation speed (*b*) density-weighted displacement speed and (*c*) curvature of the stably propagating single-cusp flame front defined by the $T = 1.15$ and $T = 3$ isolines. Heat conduction (*HC*) along the flame front upstream from both the stably propagating single-cusped flame and the planar flame front defined by the $T = 3$ isoline: (*d*) total *HC*, (*e*) normal and (*f*) tangential components of *HC*.

the colder mixture upstream of the flame. For $Le = 1$ flames, the relative effect of the focusing of heat (dependence of HC_n on curvature) on the variation of the total heat conduction along the flame is weaker than that of HC_t: along the $T = 3$ isoline, HC_t contributes approximately 80 % to the variation of heat conduction along the flame. However, the value of the total heat conduction is dominated by HC_n.

The divergence of the stream lines upstream from the convex flame segment results in a reduction of the flow velocity ahead of the flame. In addition, the effect of curvature on thermal conduction leads to a reduced displacement speed of the convex segment in comparison to the speed of the planar front. On the contrary, the convergence of the flow streamlines at the concave part reflects an increase in the incoming flow velocity which balances the increased displacement speed of the flame front. During stable propagation, the flame acquires the shape which balances the variations of the flow field with the variations of the displacement speed.

The density-weighted displacement speed $\hat{S}_d$ along the $T = 3$ front was computed for the single-cusp structures in all cases considered. The values of $\hat{S}_d$ at the flame trailing and leading points are plotted in figure 6(*a,b*), respectively. The single-cusp structure is stable in the h_{10} and h_{20} domains and the extracted values are valid after the initial transient. In the h_{40} and h_{80} domains, the values plotted are at time instants $t = 257$ and $t = 252$, respectively, when the flame acquired the single-cusp shape. At the concave segment, $\hat{S}_d$ increases with h, following the continuous increase of curvature (figure 6*a*), solely due to the influence of the flame geometry on the upstream heat conduction. On the other hand, as the domain height is increased, the curvature at the convex part diminishes asymptotically to the zero value of the planar flame, and $\hat{S}_d$ tends to the value of the planar front (figure 6*b*). The low curvature at the convex segment and the resulting low stretch rates cannot stabilize high wavenumber modes and small-scale cells appear. The important point though is that at long times these cells move towards and are annihilated at the trough with the flame acquiring again its single-cusp structure.
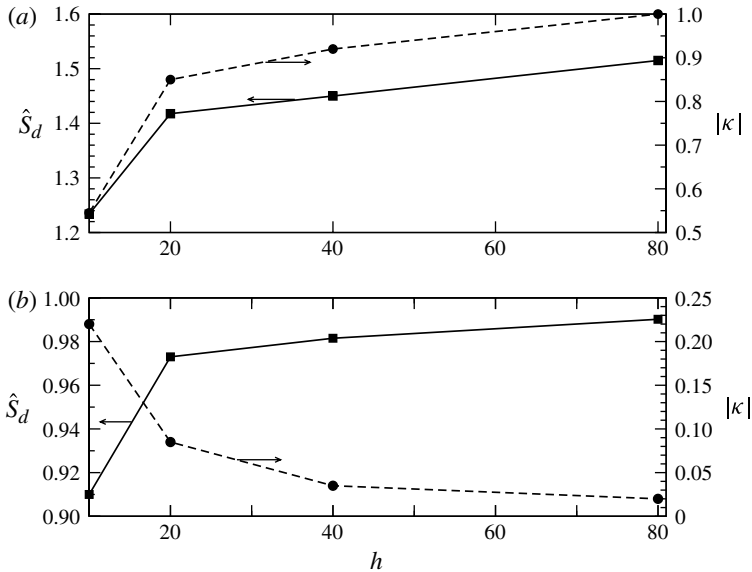
FIGURE 6. Displacement speed and curvature of (*a*) the concave (trough) and (*b*) the convex (crest) part of the single-cusp shape flame.

The effect of the domain height on flame surface area and propagation rate is summarized in figure 7. The flame surface area, L_f, defined as the arclength of the $T = 3$ isoline when the single-cusp shape is obtained, increases linearly with the domain height as $L_f = a(h - h_c) + h_c$ with $a = 1.285$ (figure 7*a*), where the stability threshold determined by the linear stability analysis is $h_c = 9.08\delta_T$. For $h \leqslant h_c$, the flame area increases as $L_f = h$, as indicated by the dashed line which is extrapolated to $h = 80\delta_T$ in figure 7(*a*). The normalized increase of L_f with respect to the domain height, $d_L = (L_f - h)/h$ at the limit of large h is then

$$\lim_{h \to \infty} \frac{L_f - h}{h} = \lim_{h \to \infty} \frac{h(a-1) - h_c(a-1)}{h} = a - 1, \tag{3.1}$$

a being the slope determined above. The value determined by (3.1) to be approximately 28.5 % establishes an asymptotic upper limit for d_L.

The normalized increase of the global displacement rate $U = (S_D - S_L)/S_L$ shown in figure 7(*b*) follows the same trend as d_L and increases asymptotically to the value determined above. This results in an upper limit for both the global propagation and global displacement rate that becomes independent of the domain height (figure 7*c*). The global displacement rate is equal to the ratio of the actual flame length to the domain height, $S_D \equiv L_f/h$. The bifurcation at $h = h_c$ marking the transition from the stable planar flame to the accelerated single-cusped flame (figure 7*b*) is in close quantitative agreement with the results of Creta & Matalon (2011).

An upper limit for the increase of the global displacement rate of stationary curved flames was also predicted in the studies of Bychkov (1998), who took into account the effects of thermal expansion in a weakly-nonlinear model first proposed by Sivashinsky (1977*a*), and with the thin flame studies of Rastigejev & Matalon (2006*a*), and more recently by Creta *et al.* (2011) and Creta & Matalon (2011) taking into account realistic density variations. Our results agree well with Bychkov (1998), where
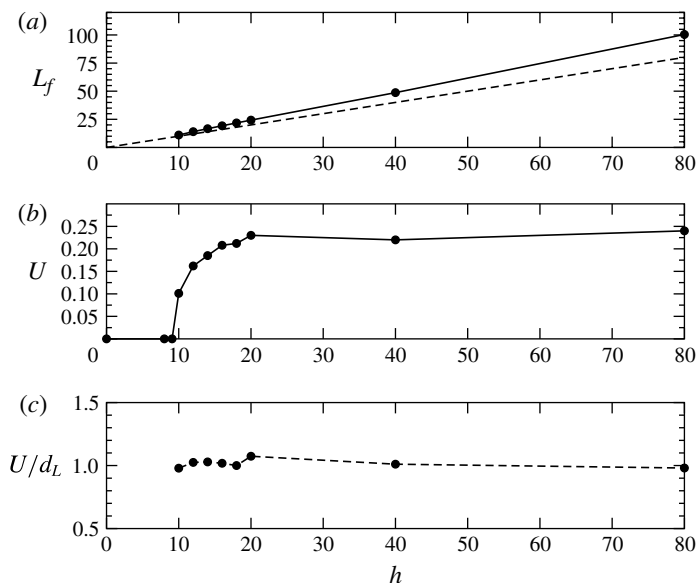
FIGURE 7. Effect of the domain height on (*a*) flame length, (*b*) increase rate of the global displacement rate $U = (S_D - S_L)/S_L$, and (*c*) ratio of the increase rate of the global displacement rate over the flame length increase normalized by the planar flame length.

the asymptotic limit of the increase of the global displacement rate is around 28 % for expansion coefficient $\sigma = 6.2$. The upper limit of Rastigejev & Matalon (2006*a*) was approximately half the one computed here, while the incorporation of the effect of hydrodynamic strain on the flame propagation speed by Creta *et al.* (2011) resulted in values closer to the ones obtained here with the upper limit for a flame with $\sigma = 5.5$ being 24.5 %. The ratio of the propagation rate to d_L is very close to unity for all domain heights considered, indicating that in $Le = 1$ flames the propagation rate reflects the normalized increase of the flame area.

Earlier theoretical studies of Vaynblat & Matalon (2000*a*,*b*) predicted that for Lewis number larger than Le_{eff}^*, the flame acquires a single-cusp stably propagating structure for any domain size. This prediction was initially proved for weak-thermal expansion and later confirmed for realistic density variations in numerical studies (Rastigejev & Matalon 2006*a*; Creta & Matalon 2011), based on a fully-nonlinear hydrodynamic model but with the flame treated as a surface of density discontinuity. It was shown that secondary modes are amplified and smaller structures can appear as a result of numerical noise, but these small-scale structures were not sustained during propagation and they finally disappear at the cusp. The results of the current study, which resolves the finite flame thickness are in agreement with these predictions, at least for the domains considered $h \leqslant 80\delta_T$.

3.2.2. *Thermodiffusivelly and hydrodynamically unstable flames*

In this case, the combined effects of the hydrodynamic and the thermodiffusive instabilities lead to intensification of the reactivity at positively-curved and weakening at negatively-curved segments. The locally increased reactivity and the modification of the flow field due to thermal expansion result in flattening of the positively-curved

segment, rendering it susceptible to perturbations of lower wavelength and leading to the formation of small-wavelength cells along the flame front.

After the initial linear growth, secondary modes are amplified as the flame crest starts to flatten. The increased curvature at either side of the crest results in intensification of the thermodiffusive effects, higher local reactivity at the crest edges, and its broadening at the expense of the trough. Depending on the domain height, when the crest is flat enough to become unstable with respect to perturbations with wavenumbers higher than that of the initial mode, the initial crest splits into two smaller cells whose tips are the edges of the initial cell. This cell-splitting is a typical pattern formation mechanism in thermodiffusively unstable flames when hydrodynamic effects are not taken into account (Denet & Haldenwang 1992; Kang, Baek & Im 2006).

Figure 8 shows the propagating $T = 3$ isoline and the corresponding time history of the HRR. In the h_3 domain (not shown), the flame remains planar and stationary during time integration for 200 time units. In the $h_{3.5}$ domain, the planar flame becomes unstable and after a transient period of linear growth a single cell forms which maintains its shape and propagates at constant speed towards the inflow (figure 8a), a behaviour that can also be inferred from the HRR signal (lower plot of figure 8a). Along the front, the influence of curvature on the reactivity is significant even in narrow domains and the HRR at the crest edges is approximately 40 times larger than at the trough.

Owing to this non-uniformity of the reactivity along the flame, the propagation rate of the flame when it acquires its final shape is no longer related only to the flame area. For the $h_{3.5}$ domain, the global displacement rate is $S_D = 2.68S_L$, while the increase of the flame area is only $\sim 47\%$ (figure 9a). The global displacement rate of the stably propagating flame is approximately 43% larger than the upper limit assessed previously for the $Le = 1$ flames. This can be understood by comparing the density-weighted displacement speed (figure 9b) and the curvature (figure 9c), with the corresponding values of the $Le = 1$ flame (figure 5). Curvature is larger in absolute value along the low Le flame, strongly affecting heat conduction upstream of the flame and resulting in the higher values of $\hat{S}_d$ along both the concave and the convex regions. In the concave region, the influence of curvature on heat conduction leads to higher values of $\hat{S}_d$. In the convex region, although the positive curvature effects tend to decrease the displacement speed below S_L, the observed values remain higher than the laminar flame speed as a result of the increased reactivity.

In the h_4 domain, the tip flattens further and the reactivity at the lower cell edge is intensified more than at the upper, eventually leading to loss of symmetry (figure 8b). The asymmetric cell acquires a lateral velocity component and the cell propagates with a constant global propagation rate of $0.8S_L$ and $2.77S_L$ in the lateral and streamwise direction, respectively. The numerical investigation of the lateral flame movement by Kadowaki (1997) showed that it occurs in $Le < 1$ flames over a narrow range of domain heights. Neither curvature nor $\hat{S}_d$ differ substantially at the cell edges in figure 9(d–f), where the negatively curved region corresponds to the cusp and the two local minima of $\hat{S}_d$ mark the cell edges. In contrast, the variation of S_a is large at the edges reflecting the significant effect of cell formation on the flow field. Since S_a is varying strongly along the flame in comparison to the displacement speed, the term that contributes to the modification of S_a is the normal component of the flow velocity.

As h is increased further, the dynamical behaviour of the flame is enriched by the appearance of interacting high-wavenumber modes. Following the formation of the
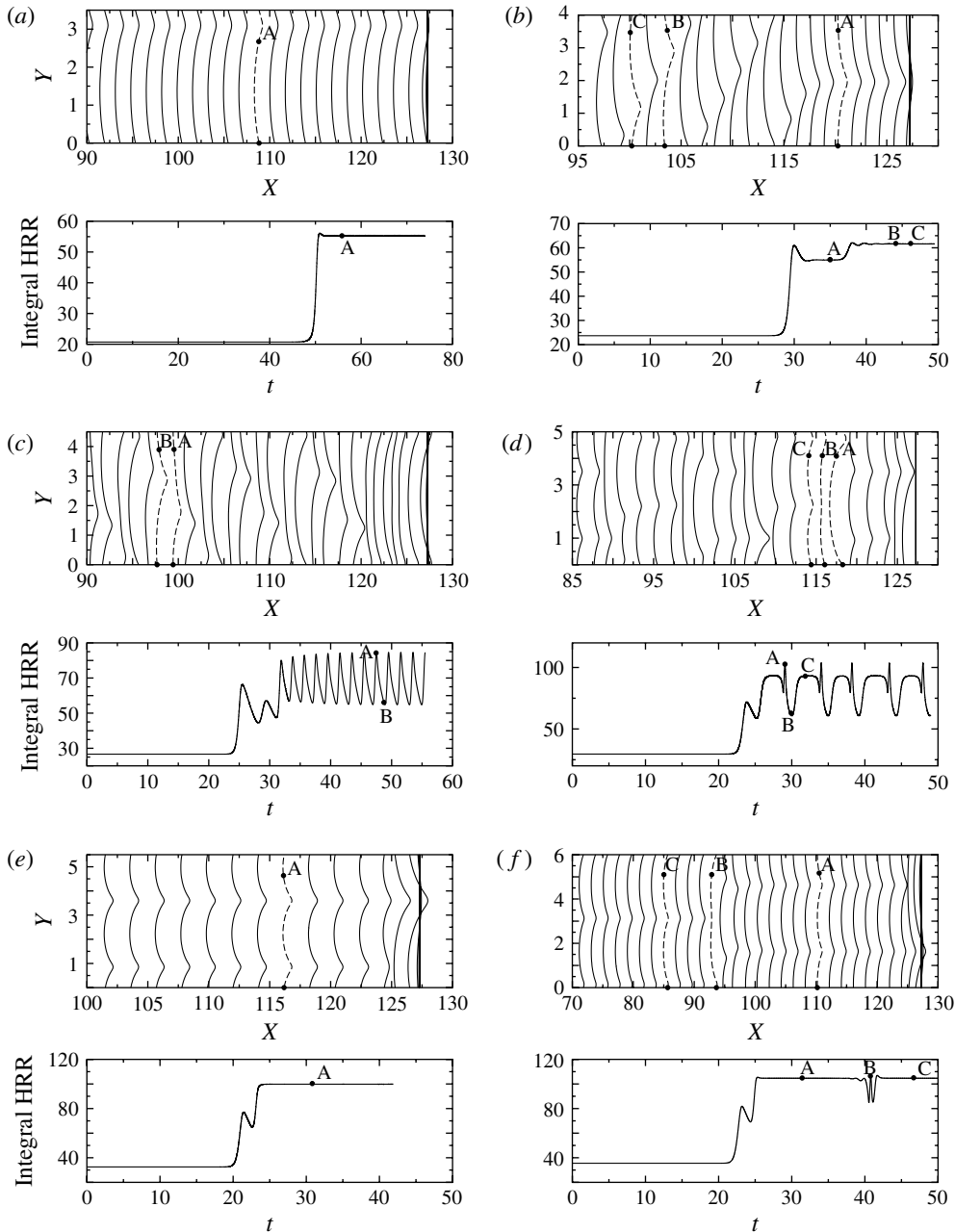
FIGURE 8. Propagation of the $T = 3$ isoline for $Le_{eff} = 0.404$ at times differing by one time unit (upper plot) and temporal evolution of the integral heat release rate (lower plot): (a) $h = 3.5\delta_T$; (b) $h = 4\delta_T$; (c) $h = 4.5\delta_T$; (d) $h = 5\delta_T$; (e) $h = 5.5\delta_T$; (f) $h = 6\delta_T$.

larger cell in the $h_{4.5}$ domain, and while the flame propagates toward the unburnt mixture, the single HRR maximum is split into two and two regions of increased reactivity appear at the sides of the crest. Since the domain is too low to allow secondary modes to develop fully, the dynamics of the flame are determined by the
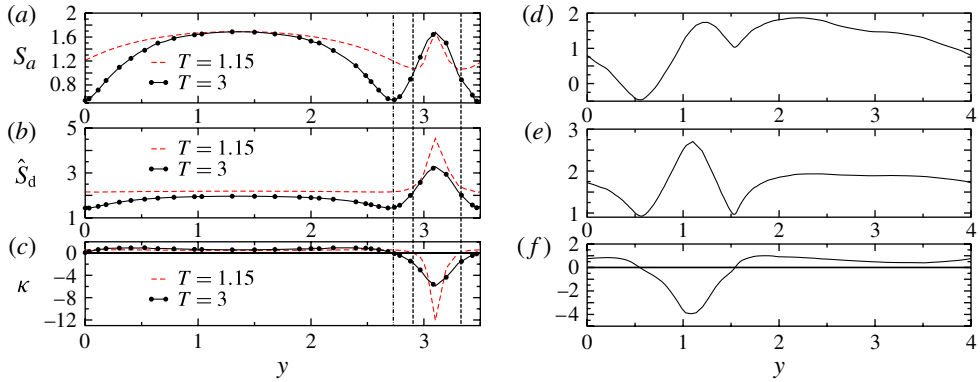
FIGURE 9. (Colour online) Thermodiffusively unstable flames: normal component of (*a,d*) the absolute propagation velocity, (*b,e*) density-weighted displacement speed and (*c,f*) curvature of the stable single-cusp flame. (*a–c*) Flame defined by the $T = 1.15$ and $T = 3$ isolines in the $h_{3.5}$ domain. (*d–f*) Flame defined by the $T = 3$ isoline in the h_4 domain.

interaction of the k_1 and k_2 modes. After two oscillations of the symmetric flame ($25 \leqslant t \leqslant 32$) during which the region of increased reactivity shifts to the crest sides, the further increase of the reactivity at the upper cell edge results in symmetry breaking and induces lateral movement of the oscillating front. In contrast to the h_4 case, and as indicated by the oscillatory profile of the HRR signal (figure 8*c*), the lateral velocity varies as the flame oscillates between an almost symmetric and an asymmetric shape. The maximum temperature varies between 2115.8 K (asymmetric flame) and 2050.2 K (almost symmetric flame).

Symmetry-breaking phenomena are characteristic of diffusionally imbalanced flames since they are a consequence of the variable reactivity along the flame. As discussed in the previous section, perturbations of the cellular front of $Le = 1$ flames are corrected by the modification of the displacement speed due to curvature effects and finally disappear at the trough. In thermodiffusively unstable flames, the perturbation on the front leads to the additional modification of the reactivity, which in turn results in local intensification of the reaction in convex parts and further increase of the displacement speed, thus amplifying the perturbation.

The narrowest simulated height that allows two distinct cells to appear is $h = 5.0\delta_T$. During propagation, one of the cells increases at the expense of the other, leading to the formation of a short-lived single cell, which quickly splits again into two in a quasi-periodic manner (figure 8*d*). During the nonlinear interaction of the unstable modes, the wavenumber of the cells formed after splitting is temporarily higher than the critical wavenumber obtained by the dispersion relation.

In the $h = 5.5$ domain, the dominance of the secondary mode results in the formation of a two-cell flame structure that propagates stably as shown in figure 8(*e*). Once formed, the two-cell flame remains unchanged and the identical cells have wavenumbers larger than the stability threshold obtained by the linear stability analysis. The global displacement rate in this case is $S_D = 3.1S_L$, while the area increases by only $\sim 52.5\%$. Formation and propagation of a two-cell flame is also observed in the $h = 6\delta_T$ domain (figure 8*f*). In this case, however, the two-cell structure propagates for $25.8 < t < 38.1$ until a short-lived single cell forms. This cell splits again to return to a two-cell structure ($t > 42.5$) which has the same propagation rate as before the
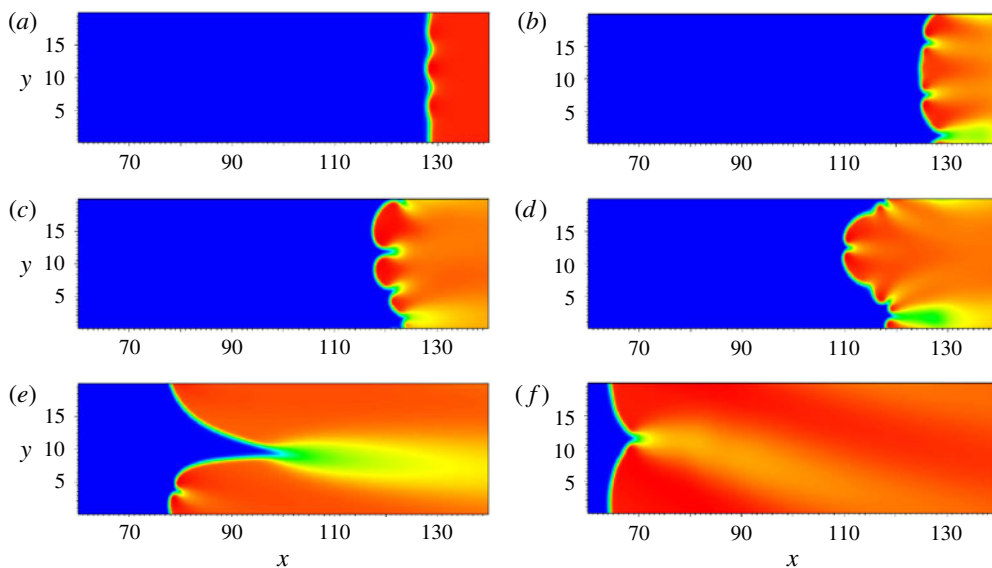
FIGURE 10. (Colour online) Isocontours of temperature of the flame propagating in the $h = 20\delta_T$ domain at (*a*) $t = 20$, (*b*) $t = 22.4$, (*c*) $t = 27$, (*d*) $t = 30.2$, (*e*) $t = 40$ and (*f*) $t = 48$ ($Le_{eff} = 0.404$).

merging and splitting. Owing to the long time interval needed for the appearance of the single cell, it was not possible to check whether the merging–splitting process is periodic.

In larger domains ($h \geqslant 10\delta_T$), the effect of hydrodynamic instability is even more significant, while the stabilizing effect of transverse diffusion weakens. In contrast to all previous cases where either periodic or stable patterns appeared, the nonlinear propagation regime is characterized by the interaction of a larger number of modes. After the initial linear growth of the disturbance, the number of cells that form is equal to the integer multiple of the most unstable mode that can be accommodated in the domain. During propagation, the small cells merge increasing their wavelength, and the cell-merging process continues until large-scale structures are formed as will be discussed below.

In the $h = 20\delta_T$ domain, three cells form initially (corresponding to $\approx 20/6$ cells with the highest growth rate that can be accommodated, figure 10*b*), which, following a transient merging process result in a single cusped-like structure, (figure 10*d*). This structure propagates stably for a short period of time, until one of the two cells disappears at the through and the flame acquires a single-cusp shape (figure 10*f*), which is short-lived since the front curvature is low and thus more susceptible to instabilities. Similar behaviour was reported by Yuan *et al.* (2005) in domains with height equal to $3\lambda_{max}$, which is close to our $h = 20\delta_T$ domain. The dominance of the k_1 mode is shown in figure 11(*a*); modes of lower wavelengths prevail only for short time intervals immediately after the early growth stages of the imposed perturbation. Similar behaviour was observed for the flame propagating in the h_{40} domain.

In the largest domain considered in this study, 13 ($\approx 80/6$) cells form initially (figure 12*a*). During propagation, the cells merge until two large structures appear
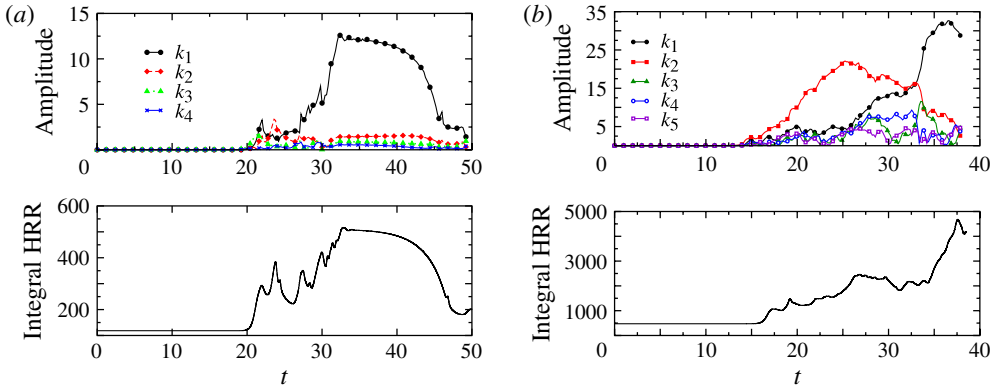
FIGURE 11. (Colour online) Time history of (*a*) the first four Fourier modes and of HRR in the h_{20} domain, (*b*) the first five Fourier modes and of HRR in the h_{80} domain ($Le_{eff} = 0.404$).

at $t \sim 30$ (figure 12*d*). Subsequently, these also merge to form a single cusped-like structure propagating towards the inflow with a large number of smaller cells appearing along its sides where curvature and stretch rate are low (figure 12*f*). The wavelength of the cells appearing along the sides is approximately equal to the wavelength exhibiting the highest growth rate, $\lambda = 6\delta_T$. Similar results concerning the characteristic wavelengths of the emerging cellular structures were reported in the experimental study of Bradley *et al.* (2000), which considered thermodiffusively unstable spherically expanding flames. The temporal evolution of the amplitudes of the first five modes together with the time history of HRR is shown in figure 11(*b*). The dominant influence of low-wavenumber modes k_1 and k_2 can be clearly seen. The k_2 mode exhibits the highest amplitude until the k_1 mode prevails. The considerable growth of the amplitude of this mode is reflected in the steep increase of the integral heat release rate occurring at the same time, i.e. around $t \sim 33$. The dominance of the first two modes, corresponding to cusped-like structures, during the nonlinear evolution of $Le = 1$ flames was discussed in the previous section. The simulation results presented in this section suggest that this is also the case for $Le < 1$ flames at long times. While in our study the dominance of the k_1 mode and the subsequent single-cell structure is always present after the initial transient, the simulations of Kadowaki *et al.* (2005) of a flame with $Le = 0.5$ propagating in a similarly large domain, showed that this single-cell structure is sustained only for small time intervals. It should be noted that because of the different choice for the reference length (l_{th} instead of δ_T), the total time simulated in the two studies is comparable.

3.3. *Effect of flame stretch on S_d*

As discussed in § 2.4, the local stretch rate can be computed using two expressions. While the total stretch rate is the same, the different terms appearing in these expressions provide interesting additional information. Figure 13 was constructed from the results along the $T = 3$ isoline of the $Le = 1$ flame propagating stably in the h_{20} domain. As expected, the two expressions for the stretch provide the same total stretch (figure 13*a*). In the laminar flow considered here, wrinkling of the front results solely from the intrinsically unstable nature of the flame. Since the stretch rate sign is the same as that of the local rate of change of the frontal area, the stretch rate is positive along the crest and negative along the trough.
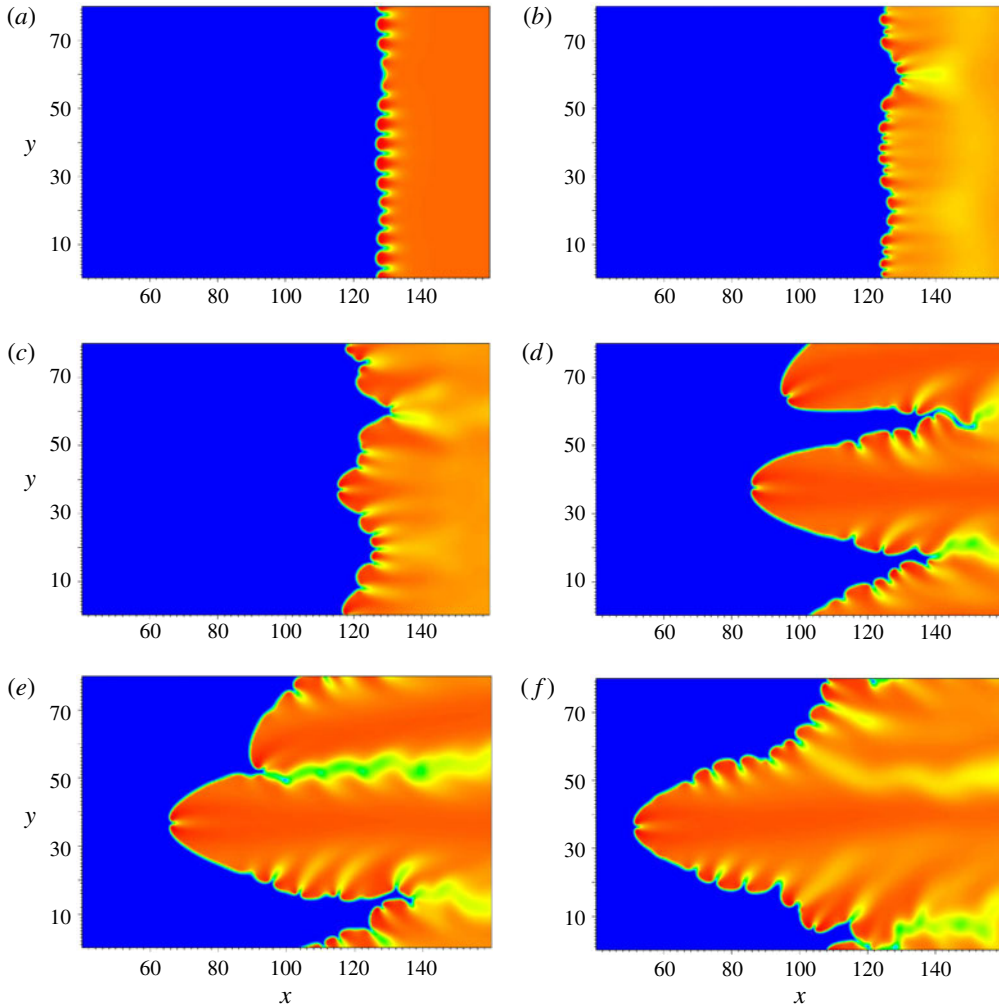
FIGURE 12. (Colour online) Isocontours of temperature of the $Le_{eff} = 0.404$ flame propagating in the h_{80} domain at (*a*) $t = 16.6$, (*b*) $t = 18.6$, (*c*) $t = 21.2$, (*d*) $t = 30.6$, (*e*) $t = 39.0$ and (*f*) $t = 44.6$.

The individual contributions of the strain rate and curvature on the total flame stretch computed using expressions (2.27*a,b*) are plotted in figure 13(*b,c*), respectively. Curvature effects expressed by the $S_d \kappa$ term are larger in absolute value than the total flame stretch, particularly along the concave regions where curvature is an order of magnitude larger. Since the flame propagates in a laminar flow, the contribution of aerodynamic strain is much lower than curvature. Expression (2.27*b*) on the other hand shows that the relative influence of the divergence of the tangential flow velocity term incorporating the dominant curvature effects is much more significant than the term expressing the effect of flame motion.

It should be pointed out that for the $T = 3$ isoline, a_t is negative along the convex and positive along the concave front segments. This variation seems counterintuitive at first, since divergence (convergence) of the flow streamlines upstream from
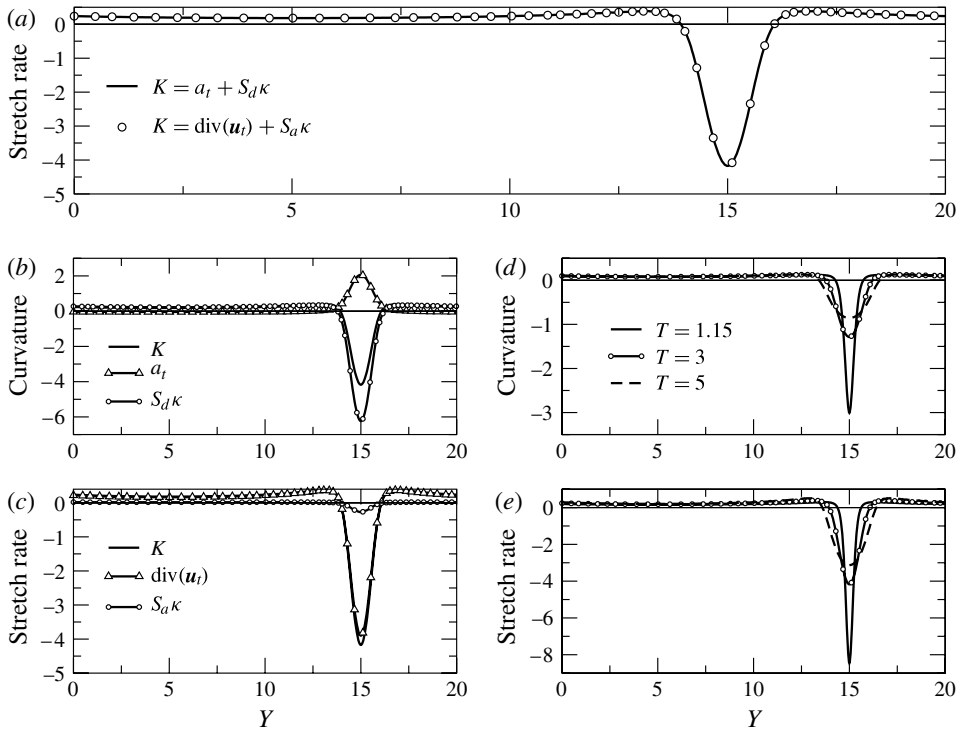
FIGURE 13. Unity Le flame front in the h_{20} domain defined by the $T = 3$ isoline: (*a*) stretch rate along the flame computed by (2.27*a,b*); (*b,c*) variations of the terms constituting the total stretch rate along the flame; (*d,e*) dependence of curvature and stretch on the definition of the flame front (variation across the flame).

the positively (negatively) curved segments would be expected to produce positive (negative) aerodynamic strain. However, for the finite-thickness flames considered here, this behaviour depends on the isoline chosen to define the front (figure 14): far upstream from the reaction zone ($T < 1.2$ region to the left of the solid line in figure 14), the streamlines diverge (converge) ahead of the convex (concave) region. In order to ensure mass and momentum conservation across the flame, the reverse is true as the flow approaches the reaction zone ($T > 3.5$ region to the right of the dashed line in figure 14).

In addition to the variation of the aerodynamic strain across the flame, flame stretch is also modified through the variation of both S_d and κ. The combined effect of the two terms results of (2.27*a*) in the dependence of the total stretch on the isoline chosen to define the flame. As shown in figure 13(*d,e*), the variation of stretch rate across the flame follows that of curvature, confirming the weak effect of aerodynamic strain on the flame propagation. Downstream of the $T = 3.5$ isoline, the variation of curvature and stretch rate across the flame is not significant, and the relation between the displacement speed and the above-mentioned quantities (expressed by the Markstein number) does not show significant variation. Concerning the variation of stretch rate along the flame front, there is no qualitative difference between unity and subunity Le flames that propagate stably. However, since $Le = 1$ flames are subjected only to hydrodynamic instabilities, the wrinkling of the front is low and stretch effects are moderate.
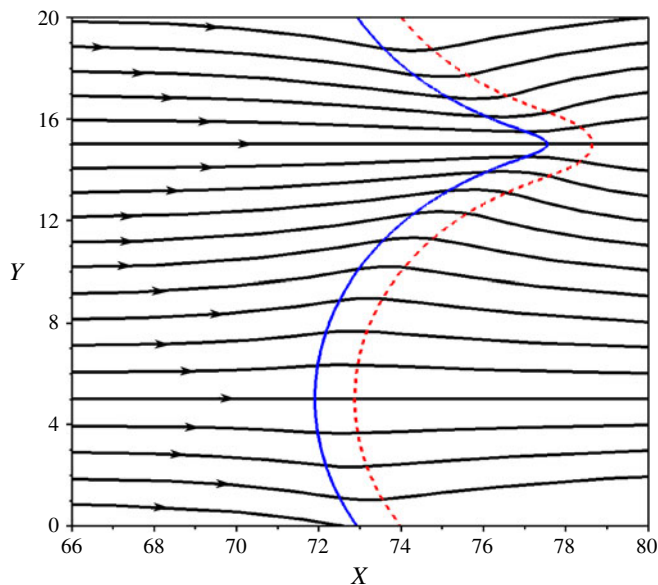
FIGURE 14. (Colour online) Streamlines of the flow field in the h_{20} domain showing the modification of the aerodynamic strain across the flame ($Le_{eff} = 1$, temperature isolines: $T = 1.2$ (solid line) and $T = 3.5$ (dashed line)).

The dependence of the density-weighted displacement speed of the $T = 3$ isoline and the normal component of the absolute propagation speed of the hydrodynamically unstable flames propagating in the h_{20} and h_{80} domains on curvature and stretch rate are plotted in figure 15. Since in this case reactivity remains constant, $\hat{S}_d$ varies linearly and monotonically with curvature reflecting the linear relation of heat conduction with curvature (figure 15a). On the other hand, due to the incorporation of aerodynamic strain, the relation between $\hat{S}_d$ and stretch rate (figure 15b) deviates from linearity. In addition, for $K \geqslant 0$ the displacement speed is not a single-valued function of the stretch rate. This is due to points along the flame front which exhibit the same $\hat{S}_d$ but experience different stretch rate due to different aerodynamic strain.

The interaction of the laminar flow field and the hydrodynamically unstable flames is shown in figure 15(c,d). No qualitative differences are observed between the relation of S_a with curvature and stretch rate. The minimum value of S_a is obtained at zero curvature. At the negatively curved region, S_a increases with the absolute value of curvature, as does the flow velocity, due to the contribution of the positive tangential heat conduction. In contrast, the decreased flow velocity upstream from the convex flame segment is balanced by the reduced displacement speed resulting from the negative tangential heat conduction. The equality of the S_a values at the leading point of the crest (lowest $\kappa < 0$) and the trailing point of the trough (highest $\kappa > 0$) can be clearly seen. Along the flame, the values of S_a are larger for the flame propagating in the h_{20} than in the h_{80} domain. Since the values of $\hat{S}_d$ are the same for the two cases, the difference in the S_a values results from the influence of the flow velocities via the flame curvature. The curvature profile along the $T = 3$ isoline in the narrow domain is steeper. Thus, through the effect of the hydrodynamic instability the larger divergence (convergence) of the streamlines upstream from convex (concave) regions reflects the intensified variation of the flow field upstream from the flame front.
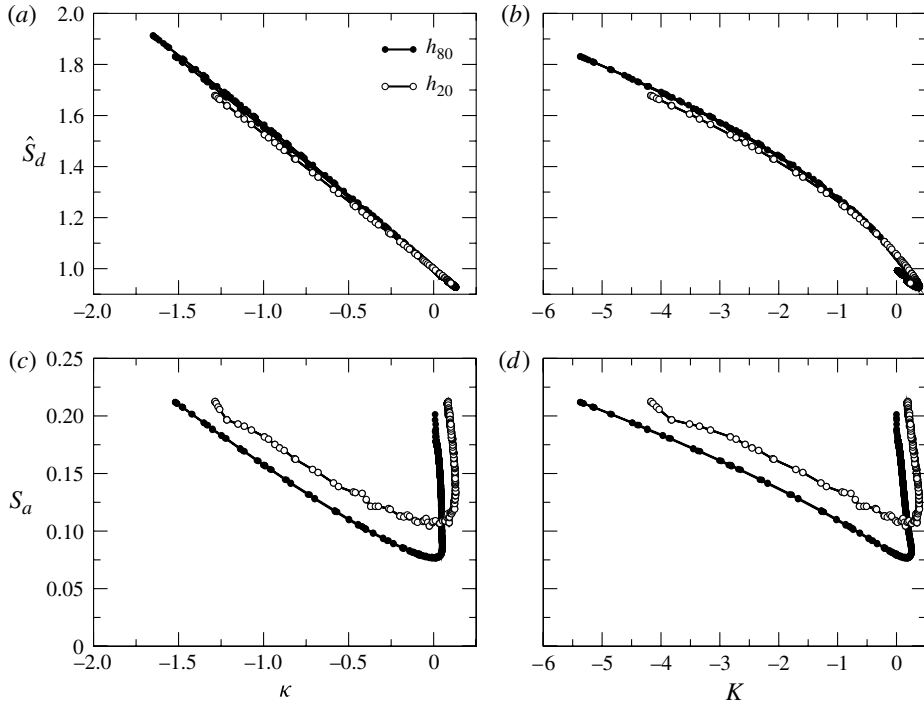
FIGURE 15. Dependence of (*a*,*b*) the density-weighted displacement speed and (*c*,*d*) normal component of the absolute propagation velocity on curvature and stretch rate, respectively, in the h_{20} (open circles) and h_{80} (filled circles) domains ($Le = 1$, flame front defined by the $T = 3$ isoline; the h_{80} data are at $t = 255$ and 285).

The effect of thermodiffusive instability is presented in figure 16, plotting the heat release rate, $\hat{S}_d$ and S_a versus curvature and stretch rate for the stably propagating single-cell flame in the $h_{3.5}$ domain (open circles) and the flame propagating in the h_{80} domain at representative time instants (filled circles). The appearance of small-scale cellular structures together with the variation of reactivity play a crucial role in the modification of the local propagation characteristics of the flame. The relation of reactivity with curvature and with stretch rate plotted in figure 16(*a*) clearly shows that increased curvature enhances burning intensity and the reactivity at the crest ($\kappa > 0$) is orders of magnitude larger than at the trough ($\kappa < 0$).

Despite the weakened reactivity at the trough, $\hat{S}_d$ increases due to the contribution of heat conduction, (figure 16*b*,*e*). Furthermore, the relations between $\hat{S}_d$ with curvature and stretch rate are not monotonic, as it is found to be negatively correlated with negative curvature/stretch and positively correlated with positive curvature/stretch, reflecting the effects of heat conduction and reactivity. The minimum value of $\hat{S}_d$ occurs around the zero curvature region. Large scattering of the values in the wider domain is observed, stemming from the presence of a large number of cellular structures of different wavelengths along the flame. The scattering increases as the domain height is increased, but qualitatively the correlations remain unaffected.

The flow-flame interactions plotted in figure 16(*c*,*f*) appear to be uncorrelated with curvature and stretch. Large scattering of the values appears around moderately curved regions, while the negative values for the h_{80} domain indicate that flame front
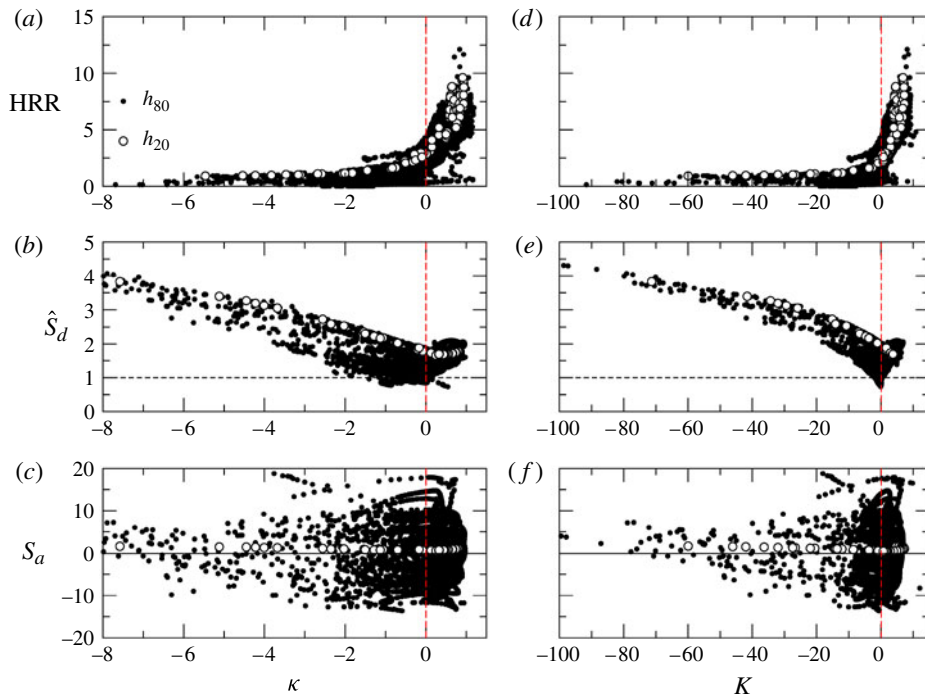
FIGURE 16. (Colour online) Dependence of (*a*,*d*) the heat release rate, (*b*,*e*) the density weighted displacement speed and (*c*,*f*) normal component of the absolute propagation velocity on curvature and stretch rate, respectively, in the $h_{3.5}$ (open circles) and h_{80} (filled circles) domains (low Le, flame front defined by the $T = 3$ isoline; the h_{80} data are at $t = 25, 30, 33$).

segments are convected downstream by the flow. Such segments are either newly formed troughs that get amplified, or small short-lived cells that cannot be sustained and are convected while they merge to form larger-scale cells.

4. Conclusions

The dynamics of propagating intrinsically unstable planar lean premixed hydrogen/air flames ($\phi = 0.6, p = 5$ atm, $T_u = 298$ K) were investigated in two-dimensional domains with heights h ranging between 3 and 80 thermal flame thicknesses. A global reaction tuned to match the laminar flame speed computed using a detailed reaction mechanism was used to describe the kinetics, and composition and temperature dependent thermodynamic and transport properties were employed in the simulations. The mixture is characterized by an effective Lewis number significantly lower than unity ($Le_{eff} = 0.404$), so that the perturbed planar flame is subjected to thermodiffusive and hydrodynamic instability. In order to understand and distinguish the thermodiffusive and hydrodynamic effects, the case of species mass diffusivities equal to the thermal diffusivity was also considered. In both cases, the initial linear growth of low-amplitude perturbations superimposed on the planar flame as well as the long-term evolution of the front were investigated.

The growth rates during the initial linear response to the imposed perturbations were computed and compared with theoretical dispersion expressions based on linear stability. In the subunity Lewis number case, the numerical growth rate curve

exhibits an inflection point at low wavenumbers and identifies the range of unstable wavenumbers ($0 \leqslant k \leqslant 1.974$) and the wavenumber of maximum amplification k_{max}. The dispersion relation obtained from the hydrodynamic theory, which properly accounts for hydrodynamic effects including gas expansion and incorporates diffusion systematically in the analysis, is a long-wave asymptotic approximation to the exact relation derived up to second order in k. As a result, the agreement between theoretical predictions and computed results deteriorate as the wavenumber k increases. Although for unity Lewis number flames both results remain qualitatively comparable, in the $Le < 1$ case the hydrodynamic theory is not able to capture the low-wavelength stabilizing diffusive effects for the mixture considered in this study and predicts an unconditionally unstable flame. On the other hand, the instability threshold is found to agree reasonably well with the predictions of the thermodiffusive theory, despite the gross simplification of constant density it presumes.

The effect of diffusive processes on the long-term dynamics of the flame was systematically investigated by varying the domain height. In agreement with the hydrodynamic theory, the hydrodynamically unstable $Le = 1$ flames acquire a single-cell structure which propagates with a constant absolute velocity towards the inflow. Owing to the low stretch rate along the convex flame segment, modes of higher wavenumber are occasionally excited, but they eventually disappear at the trough and the flame reverts to its preferred shape. On the other hand, the dynamic behaviour of diffusionally imbalanced flames was found to depend on the domain height. In narrow domains, where the thermodiffusive effects are dominant, stable or quasi-periodic structures are obtained. Lateral flame movement resulting from the locally increased reactivity at one of the crest sides and the associated loss of symmetry is observed over a narrow range of domain heights. As h is further increased, the effect of the hydrodynamic instability on flame wrinkling becomes more important, and in large domains it is the dominant mechanism. This is reflected in the dominance of the single-cusp structure of wavelength equal to the domain height, which is similar to the $Le = 1$ case. In this case, however, small-scale cellular structures form continuously along the low curvature sides of the cusp, which move towards and are annihilated at the flame trough.

The influence of flame shape on the propagation characteristics of the unstable fronts was analysed. Although reactivity remains constant along the $Le = 1$ flames, the flame propagation speed relative to the incoming flow is modified due to heat conduction and its strong dependence on flame curvature. Consequently, flame speed definitions such as the local consumption speed which is solely based on reactivity are not appropriate, and the displacement speed incorporating in addition diffusive effects should be used instead. For thermodiffusively unstable flames, both reactivity and heat conduction vary locally and their relative contribution in the local displacement speed S_d depends on the flame curvature. In positively curved (convex) regions, increased S_d results from enhanced reactivity. In concave regions where reactivity is lower by an order of magnitude in comparison to the convex regions, S_d is nevertheless higher due to the dominant influence of the tangential heat conduction. The increase of the global displacement rate S_D of the stably propagating flames over the laminar flame speed is always equal to the increase of the flame area for $Le = 1$ flames, and asymptotically reaches an upper limit of approximately 28.5 %, in good agreement with results obtained in the context of the hydrodynamic theory. In contrast, low Le flames with realistic transport in narrow domains have global flame speeds significantly larger than the corresponding flame area increase.

Finally, the effects of stretch on the propagation characteristics of the flame were studied in detail to identify the individual contributions of pure aerodynamic strain

and curvature effects. It was shown that for hydrodynamically unstable flames, the local density-weighted displacement speed $\hat{S}_d$ scales linearly with curvature, but, due to unsteady aerodynamic effects, it is nonlinearly related to stretch rate. For this case, a unique Markstein number valid for negative as well as positive curvatures can be defined. In thermodiffusively unstable flames, the dependence of reactivity on local curvature counteracts the effect of curvature on heat conduction. As a result, $\hat{S}_d$ is nonlinearly related to both stretch and curvature and, in contrast to unity Lewis number flames, it varies in a non-monotonic way. Since $\hat{S}_d$ is negatively correlated with negative curvature and positively correlated with positive curvature, different Markstein numbers should be defined in each regime.

Acknowledgements

REFERENCES

ALTANTZIS, C., FROUZAKIS, C. E., TOMBOULIDES, A. G., KERKEMEIER, S. G. & BOULOUCHOS, K. 2011 Detailed numerical simulations of intrinsically unstable two-dimensional planar lean premixed hydrogen/air flames. *Proc. Combust. Inst.* **33**, 1261–1268.

BARENBLATT, G. I., ZELDOVICH, Y. B. & ISTRATOV, A. G. 1962 On diffusional-thermal stability of a laminar flame. *J. Appl. Mech. Tech.* **4**, 21–26.

BRADLEY, D., CRESSWELL, T. M. & PUTTOCK, J. S. 2001 Flame acceleration due to flame-induced instabilities in large scale explosions. *Combust. Flame* **124**, 551–559.

BRADLEY, D., SHEPPARD, C. G. W., WOOLLEY, R., GREENHALGH, D. A. & LOCKETT, R. D. 2000 The development and structure of flame instabilities and cellularity at low Markstein numbers in explosions. *Combust. Flame* **122**, 195–209.

BYCHKOV, V. V. 1998 Nonlinear equation for a curved stationary flame and the flame velocity. *Phys. Fluids* **10**, 2091–2098.

BYCHKOV, V. V. & LIBERMAN, M. A. 2000 Dynamics and stability of premixed flames. *Phys. Rep.* **325**, 115–237.

BYRNE, G. D. & HINDMARSH, A. C. 1999 PVODE, an ODE solver for parallel computers. *Intl J. High Perform. Comput. Appl.* **13**, 354–365.

CANDEL, S. M. & POINSOT, T. J. 1990 Flame stretch and the balance equation for the flame area. *Combust. Sci. Technol.* **70** (1–3), 1–15.

CHAKRABORTY, N. & CANT, R. S. 2004 Unsteady effects of strain rate and curvature on turbulent premixed flames in an inflow-outflow configuration. *Combust. Flame* **137**, 129–147.

CHEN, J. H. & IM, H. G. 1998 Correlation of flame speed with stretch in turbulent premixed methane/air flames. *Proc. Combust. Inst.* **27**, 819–826.

CHU, B. T. & KOVASZNAY, X. 1958 Non-linear interactions in a viscous heat conducting compressible gas. *J. Fluid Mech.* **3** (5), 494–514.

CHUNG, S. H. & LAW, C. K. 1984 An invrariant derivation of flame stretch. *Combust. Flame* **55**, 1984.

CLAVIN, P. 1985 Dynamic behavior of premixed flame fronts in laminar and turbulent flows. *Prog. Energy Combust. Sci.* **11**, 1–59.

CRETA, F., FOGLA, N. & MATALON, M. 2011 Turbulent propagation of premixed fames in the presence of Darrieus–Landau instability. *Combust. Theor. Model.* **15**, 267–298.

CRETA, F. & MATALON, M. 2011 Strain rate effects on the nonlinear development of hydrodynamically unstable flames. *Proc. Combust. Inst.* **33**, 1087–1094.

DARRIEUS, G. 1946 Propagation d'un front de flamme. *Sixth International Congress of Applied Mathematics*.

DAY, M., BELL, J., BREMER, P.-T., PASCUCCI, V., BECKNERA, V. & LIJEWSKI, M. 2009 Turbulence effects on cellular burning structures in lean premixed hydrogen flames. *Combust. Flame* **156** (5), 1035–1045.

DENET, B. & HALDENWANG, P. 1992 Numerical study of thermal-diffusive instability of premixed flames. *Combust. Sci. Technol.* **86**, 199–221.

DENET, B. & HALDENWANG, P. 1995 A numerical study of premixed flames Darrieus-Landau instability. *Combust. Sci. Technol.* **104**, 143–167.

DEVILLE, M. O., FISCHER, P. F. & MUND, E. H. 2002 *High-order Methods for Incompressible Fluid Flows*. Cambridge University Press.

FISCHER, P. F., LOTTES, J. W. & KERKEMEIER, S. G. 2008 nek5000 Web page. http://nek5000.mcs.anl.gov.

FRANKEL, M. L. & SIVASHINSKY, G. I. 1982 The effect of viscosity on hydrodynamic stability of a plane flame front. *Combust. Sci. Technol.* **29**, 207–224.

GRCAR, J. F., BELL, J. B. & DAY, M. S. 2009 The soret effect in naturally propagating, premixed, lean, hydrogen air flames. *Proc. Combust. Inst.* **32**, 1173–1180.

GROFF, E. G. 1982 The cellular nature of confined spherical propane-air flames. *Combust. Flame* **48**, 51.

HAWORTH, D. C. & POINSOT, T. J. 1992 Numerical simulations of Lewis number effects in turbulent premixed flames. *J. Fluid Mech.* **244**, 405–436.

KADOWAKI, S. 1997 Numerical study on lateral movement of cellular flames. *Phys. Rev. E* **56**, 2966–2971.

KADOWAKI, S. & HASEGAWA, T. 2005 Numerical simulation of dynamics of premixed flames: flame instability and vortex–flame interaction. *Prog. Energy Combust. Sci.* **31**, 193–241.

KADOWAKI, S., SUZUKI, H. & KOBAYASHI, H. 2005 The unstable behavior of cellular premixed flames induced by intrinsic instability. *Proc. Combust. Inst.* **30**, 169–176.

KANG, S. H., BAEK, S. W. & IM, H. G. 2006 Effects of heat and momentum losses on the stability of premixed flames in a narrow channel. *Combust. Theor. Model.* **10**, 659–681.

KARLIN, V. 2002 Celular flames may exhibit a nonmodal transient instability. *Proc. Combust. Inst.* **29** (2), 1537–1542.

KEE, R. J., DIXON-LEWIS, G., WARNATZ, J., COLTRIN, M. E. & MILLER, J. A. 1996*a* A Fortran computer code package for the evaluation of gas-phase multicomponent transport properties. *Tech. Rep.* SAND86-8246. Sandia National Laboratories.

KEE, R. J., RUPLEY, F. M. & MILLER, J. A. 1996*b* Chemkin II: a Fortran chemical kinetics package for the analysis of gas-phase chemical kinetics. *Tech. Rep.* SAND89-8009B. Sandia National Laboratories.

KURDYUMOV, V. N., PIZZA, G., FROUZAKIS, C. E. & MANTZARAS, J. 2009 Dynamics of premixed flames in a narrow channel with a step-wise wall temperature. *Combust. Flame* **156**, 2190–2200.

LANDAU, L. 1944 On the theory of slow combustion. *Acta Physicochim. USSR* **19**, 77–85.

LAW, C. K. 2006 Propagation, structure, and limit phenomena of laminar flames at elevated pressures. *Combust. Sci. Technol.* **178**, 335–360.

LI, J., ZHAO, Z., KAZAKOV, A. & DRYER, F. L. 2004 An updated comprehensive kinetic model of hydrogen combustion. *Intl J. Chem. Kinet.* **36**, 566–575.

MARKSTEIN, G. H. 1951 Experimental and theoretical studies of flame front stability. *J. Aeronaut. Sci.* **18**, 199–220.

MARKSTEIN, G. H. 1964 *Nonsteady Flame Propagation*. The Macmillan Company.

MATALON, M. 1983 On flame stretch. *Combust. Sci. Technol.* **31**, 169–181.

MATALON, M. 2007 Intrinsic flame instabilities in premixed and nonpremixed combustion. *Annu. Rev. Fluid Mech.* **39** (1), 163–191.

MATALON, M., CUI, C. & BECHTOLD, J. K. 2003 Hydrodynamic theory of premixed flames: effects of stoichiometry, variable transport coefficients and arbitrary reaction orders. *J. Fluid Mech.* **487**, 179–210.

MATALON, M. & MATKOWSKY, B. J. 1982 Flames as gasdynamic discontinuities. *J. Fluid Mech.* **124**, 239–259.

MICHELSON, D. M. & SIVASHINSKY, G. I. 1977 Nonlinear analysis of hydrodynamic instability in laminar flames - II. Numerical experiments. *Acta Astronaut.* **4**, 1207–1221.

MICHELSON, D. M. & SIVASHINSKY, G. I. 1982 Thermal-expansion induced cellular flames. *Combust. Flame* **48**, 211–217.

PALM-LEWIS, A. & STREHLOW, R. A. 1969 On the propagation of turbulent flames. *Combust. Flame* **13**, 111–119.

PATERA, A. T. 1984 A spectral element method or fluid dynamics: laminar low in a channel expansion. *J. Comput. Phys.* **58**, 468–488.

PATNAIK, G., KAILASANATH, K., ORAN, E. S. & LASKEY, K. J. 1988 Detailed numerical simulations of cellular flames. *Proc. Combust. Inst.* **22**, 1517–1526.

PELCE, P. & CLAVIN, P. 1982 Influence of hydrodynamics and diffusion upon the stability limits of laminar premixed flames. *J. Fluid Mech.* **124**, 219–237.

PETERS, N., TERHOEVEN, P., CHEN, J. H. & ECHEKKI, T. 1998 Statistics of flame displacement speeds from computations of 2-D unsteady methane-air flames. *Proc. Combust. Inst.* **27**, 833–839.

POINSOT, T. & VEYNANTE, D. 2005 *Theoretical and Numerical Combustion*. R.T. Edwards, Inc.

RASTIGEJEV, Y. & MATALON, M. 2006a Nonlinear evolution of hydrodynamically unstable premixed flames. *J. Fluid Mech.* **554**, 371–392.

RASTIGEJEV, Y. & MATALON, M. 2006b Numerical simulation of flames as gas-dynamic discontinuities. *Combust. Theor. Model.* **10**, 459–481.

REHM, R. G. & BAUM, H. R. 1978 Equations of motion for thermally driven, buoyant flows. *J. Res. Natl Bur. Stand.* **83** (3), 97–308.

RUPLEY, F. M., KEE, R. J. & MILLER, J. A. 1995 PREMIX: a Fortran program for modeling steady laminar one-dimensional premixed flames. *Tech. Rep.* SAND85-8240. Sandia National Laboratories.

SHARPE, G. J. 2003 Linear stability of planar premixed flames: reactive Navier–Stokes equations with finite activation energy and arbitrary lewis number. *Combust. Theor. Model.* **7**, 45–65.

SHARPE, G. J. & FALLE, S. A. E. G. 2006 Nonlinear cellular instabilities of planar premixed flames: numerical simulations of the reactive Navier–Stokes equations. *Combust. Theor. Model.* **10**, 483–514.

SHARPE, G. J. & FALLE, S. A. E. G. 2011 Numerical simulations of premixed flame cellular instability for a simple chain-branching model. *Combust. Flame* **158**, 925–934.

SIVASHINSKY, G. I. 1977a Nonlinear analysis of hydrodynamic instability in laminar flames: I-derivation of basic equations. *Acta Astronaut.* **4**, 1177–1206.

SIVASHINSKY, G. I. 1977b Diffusional-thermal theory of cellular flames. *Combust. Sci. Technol.* **15**, 137–146.

SIVASHINSKY, G. I. 1983 Instabilities, pattern formation, and turbulence in flames. *Annu. Rev. Fluid Mech.* **15**, 179–199.

SUN, C. J., SUNG, C. J., HE, L. & LAW, C. K. 1999 Dynamics of weakly stretched flames: quantitative description and extraction of global flame parameters. *Combust. Flame* **118**, 108–128.

TOMBOULIDES, A. G., LEE, J. C. Y. & ORSZAG, S. A. 1997 Numerical simulation of low Mach number reactive flows. *J. Sci. Comput.* **12**, 139–167.

TOMBOULIDES, A. G. & ORSZAG, S. A. 1998 A quasi-two-dimensional benchmark problem for low Mach number compressible codes. *J. Comput. Phys.* **146**, 691–706.

VAYNBLAT, D. & MATALON, M. 2000a Stability of pole solutions for planar propagating flames. I. Exact eigenvalues and eigenfunctions. *SIAM J. Appl. Math.* **60** (2), 679–702.

VAYNBLAT, D. & MATALON, M. 2000b Stability of pole solutions for planar propagating flames. II. Properties of the eigenvalues and eigenfunctions with implications to flame stability. *SIAM J. Appl. Maths* **60** (2), 703–728.

WILLIAMS, F. A. 1985 *Combustion Theory*, 2nd edn. Benjamin Cummins.

YUAN, J., JU, Y. & LAW, C. K. 2005 Coupled hydrodynamic and diffusional-thermal instabilities in flame propagation at subunity Lewis numbers. *Phys. Fluids* **17**, 1063–1072.

YUAN, J., JU, Y. & LAW, C. K. 2007 On flame-front instability at elevated pressures. *Proc. Combust. Inst.* **31**, 1267–1274.